A Parallel Plate Flow Chamber to Investigate Endothelial Glycocalyx Remodeling after Pneumonectomy

This report represents the work of one or more WPI undergraduate students submitted to the faculty as evidence of completion of a degree requirement. WPI routinely publishes these reports on the web without editorial or peer review.

Submitted by:

Natasha Cruz-Calderon

Lydia Masse

Gillian Miller

Taylor Paradis

Samantha Raskind

April 28, 2022

Professor Solomon Mensah, Ph.D., Advisor
Department of Biomedical Engineering

Professor Kristen Billiar, Ph.D., Advisor
Department of Biomedical Engineering

Table of Contents

Authorship

The authors of this paper are Natasha Cruz-Calderon (NC), Gillian Miller (GM), Lydia Masse (LM), Taylor Paradis (TP), and Samantha Raskind (SR)

Section	**Subsection**	**Primary Author(s)**	**Primary Editor(s)**
1. Introduction		All	All
2. Literature Review		All	All
3. Project Strategy	3.1 Initial Client Statement	GM	TP, LM
	3.2 Technical Design Requirements	TP, GM, LM, SR	TP, LM, SR
	3.3 Engineering Standards	GM	LM, TP, SR
	3.4 Revised Client Statement	GM, TP	LM
	3.5 Project Approach	TP, SR	LM, SR
4. Design Process	4.1 Needs Analysis	GM	LM
	4.2 Design Requirements	TP, LM, NC	LM, TP
	4.3 Modeling	TP, LM	SR, LM
	4.4 Material Selection & Fabrication	TP, LM	LM, TP, SR
	4.5 Experimentation	NC, TP, LM, SR	LM, SR
5. Final Design Verification	5.1 Flow Simulation	TP	LM
	5.2 Biocompatibility Testing of Slides and Devices	TP	LM
	5.3 Verification of Controlled Fluid Flow	SR, TP	LM
	5.4 Leak Testing	NC, TP	LM, SR
	5.5 Visualization of Cell Viability-Cell Staining	TP, GM	LM, TP
6. Final Design Validation	6.1 Recap of Goals	TP	LM, SR
	6.2 Economics	LM	TP, LM
	6.3 Environmental Impact	TP	LM
	6.4 Ethical Concerns	GM, SR	LM, SR
	6.5 Health & Safety Issues	GM, NC	LM, SR
	6.6 Manufacturability	TP	LM, GM
7. Discussion		GM, TP	LM, SR
8. Conclusion		TP	LM, SR

Acknowledgments

This project would not have been possible without the enthusiasm and guidance of our advisors, Solomon Mensah, and Kristen Billiar. We would also like to extend our gratitude to Dr. Waxman for taking the time to provide us with assistance in the design of the model and accuracy of anatomical geometric values. We are also thankful to the WPI Washburn Machine Shop and the WPI Goddard Machine Shop for their help with machining of parts, as well as Marsha Rolle for her advice on material fabrication. Finally, the team would like to thank Lisa Wall, Robert Kirch, and the WPI Biomedical Engineering Department for their help and for the funding of this project.

Abstract

A pneumonectomy can result in many complications post-surgery due to the lack of a lung and the same cardiac output of blood being forced through a single pulmonary artery. However, few studies have examined the effect of changes in the shear stress magnitude on the endothelial glycocalyx post-operation. A parallel plate flow chamber capable of mimicking the pulmonary arteries before and after a pneumonectomy was developed to collect data regarding potential damage to the glycocalyx post-pneumonectomy. Flow simulations with the designed model revealed that after a left pneumonectomy, the shear stress in the right artery increases 4-fold and after a right pneumonectomy, the shear stress in the left artery increases 3-fold. For in-vitro experiments, the flow chamber allowed for physiologically relevant shear stress to be applied on human lung microvascular endothelial cells. Changes in shear stress post-pneumonectomy were investigated using immunostaining and confocal interrogation of the endothelial glycocalyx and quantified using ImageJ. Understanding how an increase in shear stress affects the endothelial glycocalyx is critical in reducing patient mortality post-pneumonectomy.

List of Figures

List of Tables

1. Introduction

A pneumonectomy is a surgical procedure during which one entire lung is removed from a patient, and the connective vessels of this lung are sealed off [1]. There are many reasons an individual might need to undergo a pneumonectomy. These include, but are not limited to, tuberculosis in the pulmonary tract, severe injury to the lung, congenital lung disease, and pulmonary cancer metastasis [1]. The majority of lung diseases can be categorized in one of two ways, as an obstructive or restrictive disease [2]. Obstructive pulmonary diseases cause impaired expiration, so air that should be exhaled is not, and becomes trapped in the lungs. Restrictive pulmonary diseases prevent the lungs from fully expanding, which leads to decreased lung volume and efficiency. The most common cause of pneumonectomy is lung cancer, which can spread quickly throughout the lungs and removing the most affected lung is often necessary to prevent metastasis [1]. Pneumonectomies may also be performed after irreparable physical trauma to the lung has occurred [1].

There are several complications resulting from a pneumonectomy that are identifiable by radiographic imaging of the chest. Complications that occur not long after the pneumonectomy procedure include pulmonary edema, bronchopleural fistula, pneumonia of the contralateral lung, empyema, and adult respiratory distress syndrome, all of which can occur concurrently [1]. Late-stage complications include recurrent disease, infection, and complications from surgical procedures such as anesthesia, or bronchopleural and esophagopleural fistula [1].

Postpneumonectomy pulmonary edema is one of the most prevalent fatal complications resulting from the procedure, affecting 2.5-5 % of patients that undergo a pneumonectomy with an 80-100% mortality rate [2]. The mechanisms that contribute to this complication are currently unknown. However, it is predicted that postpneumonectomy pulmonary edema is influenced by changes in hemodynamic pressure differentials and capillary permeability [2]. This condition is more prevalent after a right pneumonectomy which is predicted to be due to a more significant increase in pulmonary blood flow through the left lung [3]. The left lung normally functions to receive only 45% of the total pulmonary blood flow and often the extra blood flow resulting

from a pneumonectomy can put extra stress or pressure on the arteries in the lung which can lead to conditions such as pulmonary edema [2].

Our study aims to explore the effect of changes in blood flow modeled by culture media flow over cultured cells to model vascular changes post-pneumonectomy. The experimental methods outlined later in the paper discuss how cellular changes with applied pneumonectomy flow conditions were modeled in a parallel plate chamber as well as using fluid flow simulations.

2. Literature Review

2.1 Physiology of the Lungs

The lungs are the primary organ in the respiratory system. They facilitate gas exchange between the environment and the bloodstream. Oxygen enters the bloodstream and is extracted by cells from the extracellular environment to produce ATP, and carbon dioxide is expelled as a byproduct of this reaction. In terms of mechanisms, the chest wall compliance and lung compliance, which are counteractive forces inside the lungs, work together to create a negative pressure that draws oxygen inside the lungs [3]. With each breath, oxygen is transported through the capillary system within the lungs to enter the arterial system and other tissues. When the lungs have supplied the oxygen, the positive expiratory pressure created inside the lungs forces the carbon dioxide outwards. This oxygen is bound to hemoglobin or simply dissolved in the bloodstream [5]. Both lungs are divided into lobes, with the right lung having three lobes, and the left lung having only two. Each of these lobes contains over 300 million alveoli which are tiny air sacs responsible for gas exchange within the lungs. Composed of only a single endothelial layer, the alveoli exchange carbon dioxide for oxygen through diffusion through the capillaries, tiny blood vessels lining the alveolar walls [5].

To understand the structure of the vessels in the pulmonary system, it is important to discuss the function of the lungs in conjunction with the heart. After each breath, oxygen is transferred in the alveoli, and then distributed to the surrounding capillary network; this can be seen in Fig. 2.1. The newly oxygenated blood travels through the pulmonary veins, the only veins in the body that carry oxygenated blood, and into the left atrium of the heart [4]. As the atria contracts, the blood is ejected into the left ventricle. When the ventricles contract, the blood is pumped into the aortic arch, where it is distributed to the rest of the body. Deoxygenated blood returns to the heart through the veins, entering the right atrium of the heart through the vena cava [4]. The atria contracts again, and the blood is ejected into the right ventricle. As the ventricles contract, the blood is pumped into the pulmonary arteries, which are the only arteries that carry deoxygenated blood in the body and returns the blood to the lungs to become oxygenated once again [4].

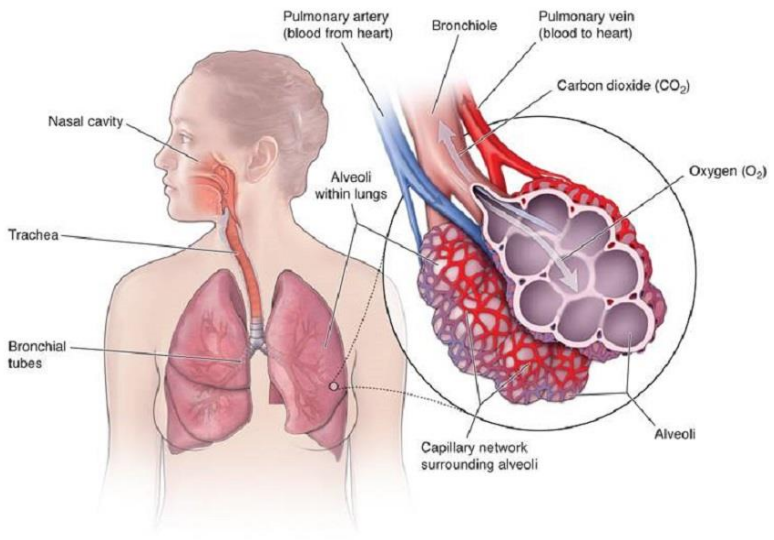

Fig. 2.1: Diagram demonstrating how the lungs exchange gas [6].

Fluids travel through the lungs in vessels that belong to one of three categories: pulmonary arteries, pulmonary veins, and capillaries. The pulmonary arteries go from the heart to the lungs, splitting at the pulmonary trunk and branching to the left and right pulmonary arteries and further branching off to form basal branches [4]. This distribution allows for the blood inside the pulmonary arteries to reach the alveoli efficiently, where it will undergo gas exchange within the capillaries. In terms of their structure, pulmonary arteries are similar to other arteries throughout the body [5]. The arterial wall is divided into three sublayers, the tunica intima, the tunica media, and the tunica adventitia. The tunica intima is primarily composed of a layer of endothelial cells, but it also includes a thinner layer of a more elastic connective tissue, helping it to attach to the outer portions of the wall. The tunica media is the thickest layer and consists of perforated elastic membranes interspersed with collagen and smooth muscle cells [5]. On the outermost side of the artery is the tunica adventitia, which is a thinner sublayer that contains connective tissue, nerves, and blood vessels. These blood vessels supply blood and nutrients directly to the artery [5].

2.2 Anatomy of the Pulmonary-Vascular System

The focus point for this study is the pulmonary arteries that are responsible for bringing deoxygenated blood from the heart to the lungs. Figure 2.2 is a diagram of the pulmonary arteries

including the main pulmonary artery, left & right pulmonary arteries, and the smaller branching arteries.

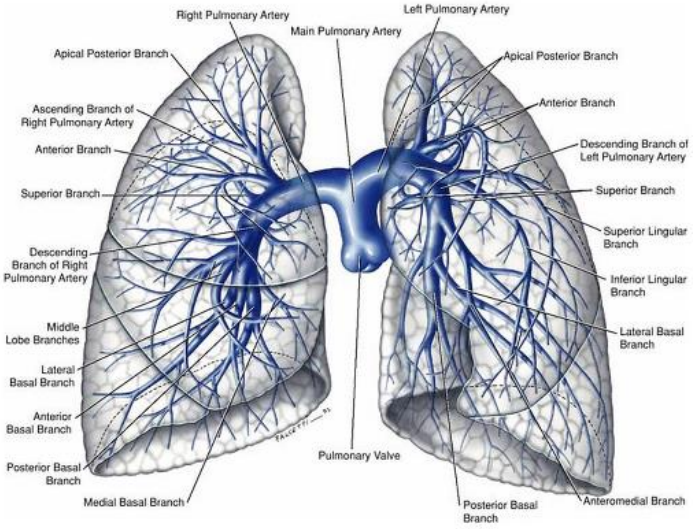

Fig. 2.2 : Diagram of the pulmonary arteries [7].

Although little information about the dimensions of the pulmonary arteries is reported outside of patient-specific case studies, a study in 2007 used multidetector contrast-enhanced computed tomography (CT) to measure the pulmonary artery diameters in healthy adults. 126 healthy adult subjects underwent thoracic CTs using a normal pulmonary artery pressure (25 mmHg). The study concluded that the upper limit diameters of the main pulmonary artery, right pulmonary artery, and left pulmonary artery are 29.5mm, 19.8mm, and 22.1mm, respectively [8].

The basal branches are segments that branch off from the pulmonary arteries into seven different branches and can be seen in Fig. 2.3. Both the right and left pulmonary arteries divide into two lobar branches and subsequently divide into segmental as well as subsegmental branches. The right lung has three lobes divided into ten segments which include the four basal segments (anterior, medial, posterior, and lateral). Conversely, the left lung has eight segments with two lobes, the lower lobe having three basal segments (anteromedial, posterior, lateral) [4]. Published literature does not go into much detail about the sizes of the basal branches, so little information is known regarding the diameters, lengths, and branching angles of the basal branches.

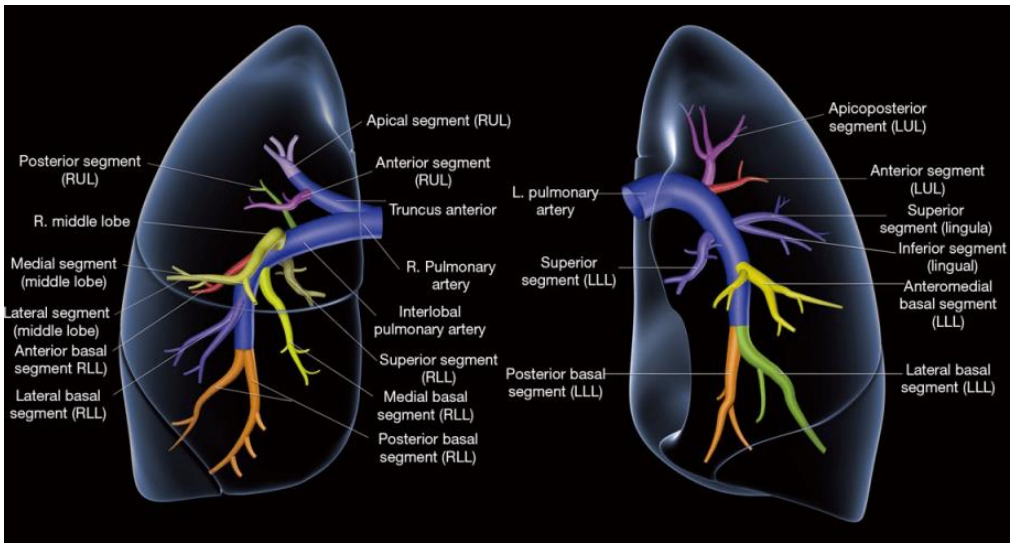

Fig. 2.3: Simplified diagram of the left and right pulmonary arteries [4].

2.3 Physiology of the Endothelial Glycocalyx

Blood vessels are composed of three layers, the tunica externa, tunica media, and tunica intima. The endothelium sits on top of the tunica intima and the endothelial glycocalyx (GCX) is adjacent to the endothelial cells. The GCX is a complex gel, a dense, porous, brush-like layer that forms an interface between blood vessel walls and circulating blood. The GCX is a mechanotransducer, with its location subjecting it to shear stress and tensile strain, and it regulates cell physiology and morphology, gene expression, and inflammatory responses [9]. The GCX thickness varies throughout the vasculature. In capillaries, they can be only a couple hundred nanometers thick, whereas in the arteries they can be a few micrometers thick [10]. This discrepancy in their thickness at different locations shows how they adapt to different nanomechanical properties in the body.

The GCX contains many components that are responsible for numerous physiological functions that are necessary for the regulation of blood pressure, control of leukocyte interactions with the endothelium, and maintenance of tissue perfusion. It is mainly composed of glycoproteins and proteoglycans. Glycoproteins perform as adhesion molecules. Cell adhesion molecules such as P-selectin, E-selectin, integrins, and immunoglobulins contribute to coagulation and hemostatic systems. Mediating platelet interacting with endothelial cells and adhesion to the endothelium [11].

The protein cores of proteoglycans are attached to glycosaminoglycan (GAG) side chains. Syndecans or glypicans will bind some of the core proteins, while others such as perlecans, versicans, decorins, biglycans, and mimecans will be secreted when GAG side chains attach to proteoglycans. Heparan sulfate (HS), hyaluronic acid, chondroitin, dermatan, and keratin sulfates are the 5 types of GAG side chains. Heparan Sulfate (HS) is one of the main components as it makes up about 50-90% of the GAG side chains. It has a role in modulating anti-inflammatory processes, controlling growth factors, and mediating chemokine gradients [12].

A healthy GCX layer is one that is subject to blood flow. Its composition continuously changes as it is made up of components that are shed into flowing blood and further along the blood vessel are reabsorbed. Blood flow helps maintain a healthy physiological balance between GCX shedding and absorption. Under prime conditions, the GXC components that are shed will flow through the bloodstream in laminar flow, and then get reabsorbed into the GXC for synthesis. However, when that flow is disturbed, the components flow away and there is no re-absorption which leads to no synthesis of new components. This will lead to the degradation of the GCX [13]. Figure 2.4 shows the endothelial glycocalyx structure for both ideal physiological conditions and under pathological conditions. The disruption of this layer can lead to cardiovascular disease which is fatal in many cases.

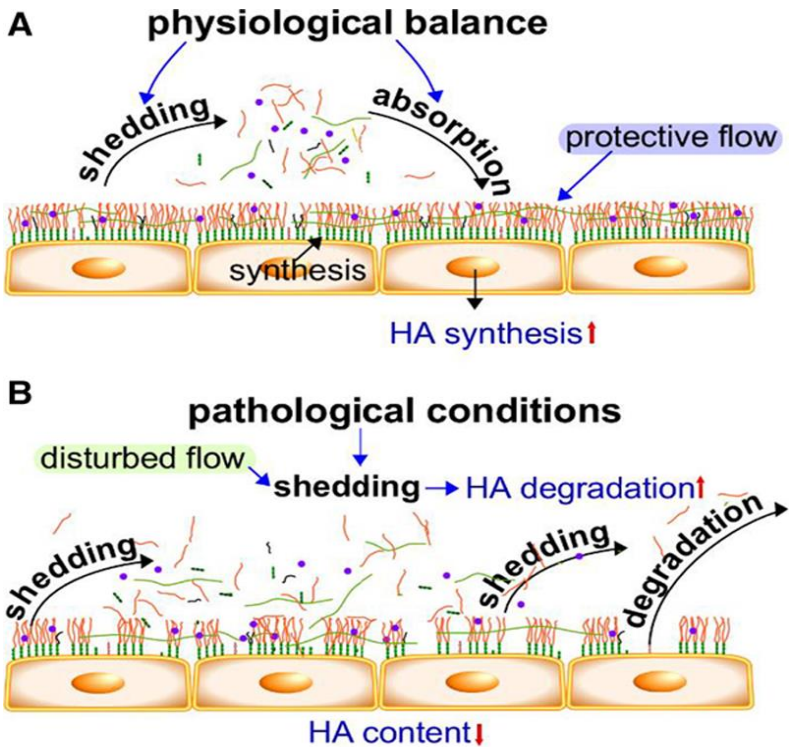

Fig. 2.44: Endothelial Glycocalyx structure. Hyaluronan (HA) is shown in light green, heparan sulfate (HS) is shown in orange, chondroitin sulfate is in dark grey, plasma proteins in purple, and glycoproteins and proteoglycans are in dark green. a) Shows the GCX under physiological conditions.) Shows GCX under pathological conditions [10].

One of the roles of the GCX is to act as a barrier. The GCX is reliant on shear stress from normal blood flow as it enhances its structure and function. The GCX can increase nitric oxide or hyaluronic oxide production as needed determined by blood flow. This increased production reduces stress on cells by activating mechanisms, like dilating the vessels. Damage to the GCX impairs this ability to protect the endothelial cells. It also protects the endothelial membrane from blood cells and other pathogens in the bloodstream from binding to it. By deterring the adhesion of particulates to the endothelial cell layer, the GCX protects the endothelial cells and maintains vascular homeostasis as it regulates vascular permeability and the interaction of molecules with endothelial receptors [14].

There are also several diseases and conditions that can cause the glycocalyx to degrade such as inflammation, trauma, hemorrhagic shock, and ischemia-reperfusion. The endothelium is part of the early systemic inflammatory response syndrome. Any damage to the GCX will prevent it from acting as a protective barrier. HS shedding increases endothelial cell sensitivity to cytokine activation [15]. Tumor necrosis factor α (TNF-α) is part of the body's immune response,

activating the release of cytokines, heparanase, histamine, and proteases will further degrade a damaged GCX. With this damage, endothelial cell adhesion becomes unregulated, triggering more inflammation and uncontrolled cell adhesion [15]. Diabetes indicates a resistance to insulin or absence of insulin, typically following high blood sugar levels, or hyperglycemia. Typically impairing the effectiveness of the GCX as a protective layer and synthesis of nitric oxide, as well as decreasing its selective permeability. A 2006 study published by the American Diabetes Association concluded that high blood sugar levels lead to a degraded glycocalyx. Also, finding the thickness of the GCX in Type-1 diabetics to be half that of the thickness in healthy controls. It also states that diabetics with microalbuminuria have an even thinner GCX. As previously stated, damage to the GCX affects the balance of shedding and reabsorption. This was observed by the elevated levels of hyaluronic acid and hyaluronidase in the plasma of diabetic patients [16].

A pneumonectomy could cause the endothelial glycocalyx to degrade immensely due to increased pressure and inflammation after a lung is removed. The degradation of the glycocalyx can lead to complications such as pulmonary edema and hypertension. To serve as a protective barrier, the glycocalyx is reliant on the forces from blood flow. A change in blood flow (or disturbed flow) will result in a change of the forces that are applied on the GCX. Changes in flow can change the patterns of GAG side chain adhesion, affecting the attachment of proteins and molecules to endothelial cell receptors, further damaging the glycocalyx, compromising its function as a protective barrier and impairing its ability to mediate responses between blood flow with the endothelial cells [17].

2.4 Pneumonectomy Procedure

A pneumonectomy procedure refers to the removal of one of the lungs. Pneumonectomies are usually performed as open-chest surgeries, as this is best for mitigation of the risks involved with surgical error. They can sometimes be performed as video-assisted thoracoscopic surgery (VATS) procedures. This involves a thoracoscope being inserted through an incision into the chest to allow surgeons to open less of the body when maneuvering medical instruments [18]. Although this is less invasive, surgeons may be hesitant to perform the surgery this way due to the high risks associated with operating via video footage. Procedurally, a

pneumonectomy begins with the surgeon creating an incision in the patient's side before cutting through the body to expose the ribs [18]. The ribs are pulled apart, and then the lung removal can occur. When the lungs are exposed, surgeons commonly use a surgical energy device, such as a cauterizing instrument, to both burn through unwanted tissue and help seal any holes left behind [18]. The surgeon must cut through the pleural adhesions, which are the pieces of fibrous tissue attaching the lungs to the inner body cavity, or pleural space. The inferior pulmonary vein is then cut, followed by the surrounding lymph nodes and any other connective tissue [18]. The pulmonary artery in question is then cut and is often stapled closed in addition to cauterization. When the lung is free it can be removed from the chest cavity. At this point, the bronchus from whichever lung is being removed can be cut away, followed by the superior pulmonary vein [18]. After some more sealing and stapling in any necessary areas, the surgeon can put a patch on the bronchial stump and begin procedures to close the chest [18]. An overview of the surgery can be seen in Fig. 2.5.

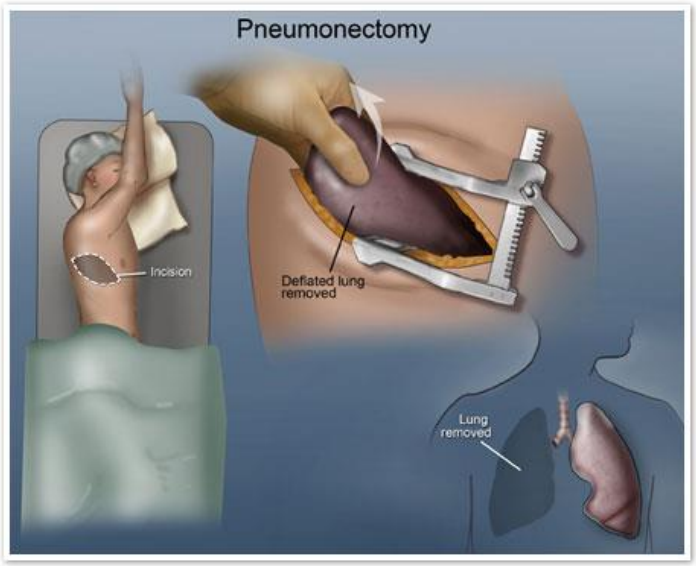

Fig. 2.55: Diagram demonstrating how a pneumonectomy is performed [19].

Figure 2.6 is an x-ray image of the chest cavity post-pneumonectomy. In this figure the left lung was removed as it can be seen missing from the X-ray.

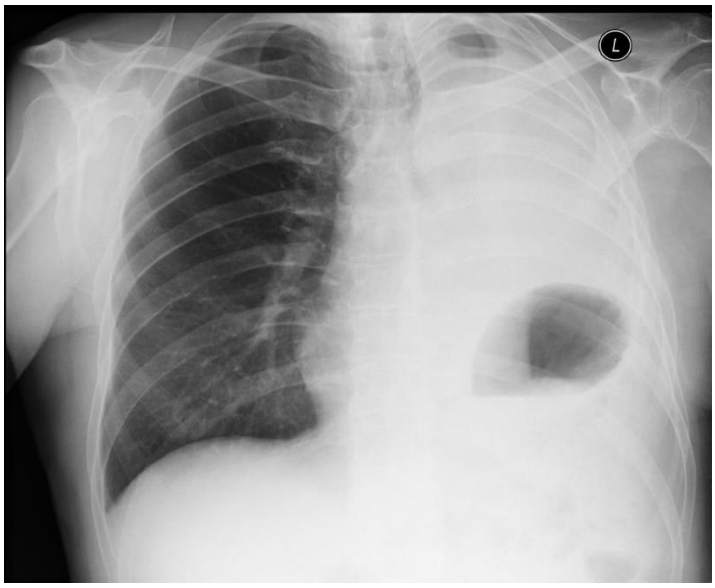

Fig. 2.66: X-ray image of lungs after a left pneumonectomy [20].

2.5 Pneumonectomy Significance

A pneumonectomy can be a life-saving procedure for patients who require a mass or growth of the lung to be removed, such as tumors due to non-small cell lung cancer and other forms of lung cancer. The removal of a lung is sometimes necessary to treat other conditions such as tuberculosis, COPD, traumatic lung injury, and congenital lung disease. Although pneumonectomies have high risks, they are still crucial in removing cancer and treating patients with other life-threatening diseases [4]. Many people can live a full and active life with only one lung, so a pneumonectomy is a potentially life-saving surgery in medicine despite its drastic result. For many people, pneumonectomy is the only potentially curative option provided, adding to its significance in the field. However, there is little research done about the effects of the increased amount of blood flowing through the one remaining artery. Instead of the blood from the heart coming up the pulmonary trunk and then being split between the left and right pulmonary arteries to either lung, all the blood is forced through one of the pulmonary arteries. The cardiac output remains unchanged because the amount of oxygen required is the same, so the volume of blood flow through the remaining pulmonary artery is doubled [17]. This unnatural flow of blood will increase the shear stress on the glycocalyx layer which can cause it

to degrade, but few studies have measured the shear stress or the rate of degradation on the glycocalyx.

2.6 Pathological Changes due to a Pneumonectomy

After a pneumonectomy, the body takes several weeks to recover and there are several postoperative complications that could occur during this time. Additionally, the pathology of the lungs and vascular system is affected by this drastic procedure. The accumulation of fluid in the area, elevation of the diaphragm, and gradual shrinking of the postpneumonectomy site are just some of the many changes that can take place after this surgical procedure. In a right pneumonectomy, organs such as the heart or liver often shift into the empty space over time. The shifting of the mediastinum can also occur, which can directly cause large airway obstructions due to the narrowing and stretching of the main bronchus [21]. The effects of pneumonectomy on the vascular system can be seen through an increase in pulmonary artery pressure and right ventricle workload [22]. An increase in pulmonary vascular resistance can follow a significant increase in blood flow which can eventually lead to pulmonary hypertension and depression of the right ventricle function [23]. A pneumonectomy can result in increased perfusion to the remaining lung and a decrease of the pulmonary vascular bed as well often leading to damage to the capillary endothelium and inflammation of the pulmonary arteries. After a pneumonectomy, the lobes of the lung may increase in weight and volume due to arterial growth. Corresponding to several postoperative conditions, there are also anatomical and pathological changes such as thorax wall deformation and progressive mediastinal displacement [24]. The hyperinflation and encroachment of the remaining lung into the postpneumonectomy space can occur and cause other organs to shift as well [21]. Pneumonectomies can also lead to pulmonary hypertension as several studies report an increase in the pulmonary artery pressure 5 years after the surgery in about a third of patients [25]. These are only a few of the known repercussions of a pneumonectomy, but since only a small population of people receive this surgery there is still a lot of research to be done.

2.7 Previous Studies

2.7.1 Blood Pressure and Flow Studies

A study performed in 1987 measured the change of the pulmonary vascular impedance along with other hemodynamic variables by performing pneumonectomies on ten dogs [26]. The primary focus of the study was to determine quantitative values for the characteristic of pressure and flow that occurs in the proximal pulmonary arteries before and after the pneumonectomy procedure. The largest observed increases were in the pulmonary vascular resistance, the work of the right ventricle, and the impedance [26]. The pulmonary vascular resistance almost doubled as the control average value was at 447 dyne*sec*cm^{-5} and then increased to 761 dyne*sec*cm^{-5}. As for the right ventricle, the mean right ventricle work increased by 0.57 J/min (16%), the oscillatory work of the right ventricle increased by 0.53 J/min (43%), and the total external work of the right ventricle increased by 1.1 J/min (23%) [26]. Lastly, the average impedance increased by 19 dyne*sec*cm^{-5}. A surprising finding from this article is that the cardiac output, which would be expected to stay the same, decreased from 1.86 L/min to 1.67 L/min [26]. This decrease can be explained by the major increase in the pulmonary vascular resistance, as the right ventricle may not be able to fully compensate for this increase [26]. While this study did not investigate the increase in shear stress or its effect on the endothelial glycocalyx layer, it describes other drastic changes that a pneumonectomy can cause on the pulmonary vascular system.

2.7.2 Cell Culture Model in Parallel Plate Flow Chamber Devices

Several studies were reviewed that investigated the effect of pulmonary artery hypertension (PAH) on cell culture through cyclic applied shear stresses on fabricated cell models, or animal models through stenting of the pulmonary artery. One such study used a microfluidic cell stretch device or parallel-plate flow chamber to imitate vascular flow and apply shear stress to examine the proliferation rates on pulmonary artery smooth muscle cells [27]. This model was representative of the effect of pulmonary hypertension, occurring after a pneumonectomy, on the arteries.

The device used in this experiment consisted of a polydimethylsiloxane (PDMS) membrane acting as the cell culture substrate and two channels, an upper cell culture channel and lower control channel, which was connected to a vacuum pump [27]. The pump applied a cyclic stretch through fluid flow pumped through channels at the frequency corresponding to a normal heart rate (80 bpm) in 0.38s intervals to replicate physiological pulmonary artery blood flow. The device simulated fluid shear stress and circumferential wall stress (cyclic stretch) to mimic the hemodynamic microenvironment of blood vessels and arteries. The results of the experiment displayed increased cell proliferation with higher applied stress on cells which was consistent with increased proliferation seen in patients with PAH [27]. It was determined that this was due to an increase in transcription rates of cyclin D1, and positive regulators contributing to human pulmonary artery smooth muscle cells (PASMC) proliferation such as hypoxia-inducible factor-1α, vascular endothelial growth factor, and transforming growth factor-β [27]. The mechanism by which this occurs is still unknown, but this study served to model vascular remodeling as a result of pulmonary hypertension and factors that contribute to this. The device allowed for the measurement of controlled applied shear stress on cell culture mimicking conditions in which this is relevant such as PAH allowing for potential explanations for this condition. This concept could be further applied to create devices to study other conditions by adding more complexity to the device to better represent the physiological system and replicate conditions.

Another study that utilized a parallel plate flow chamber was completed at the University of Pittsburgh where they used the flow chamber to investigate endothelial cell response to shear stress. This group of researchers solved the full equations of steady, three-dimensional flow in novel parallel plate devices to identify an active test region [28]. They defined this active test region as the point in the flow chamber where the shear stress is within 5% of a constant accurate value [28]. While performing their experiments the group created a uniquely designed parallel plate flow chambers with multiple testing points to study the points where the cells are exposed to nearly uniform shear stress. This paper discusses the importance of active testing regions being placed in regions that are not near the entrance of the flow chamber to allow for the inlet flow to become uniform prior to reaching the spots with cells [28]. A diagram of the parallel plate flow chamber that they designed for the research can be seen in Fig. 2.7.

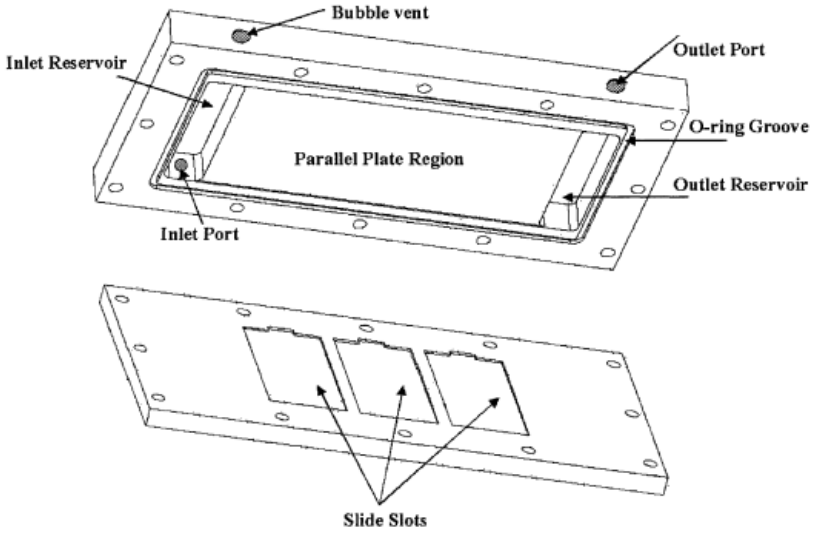

Fig. 2.77: Parallel plate flow chamber designed to determine accurate placement of cells [28].

As seen in Fig. 2.7 the flow chamber that this group created has three different slots to place glass slides. These points are where they seeded their endothelial cells for shear stress magnitude testing. In this design flow enters via the inlet port and flows into the inlet reservoir and is then forced through the labeled parallel plate flow region which includes the glass slides with cells. Fluid then exits the system by flowing into the outlet reservoir and through the outlet port. They created the two plates out of cast acrylic, and they are held together with bolts. They also included an O-ring to prevent leakage [28].

Parallel plate flow chambers are often used to study endothelial cells' responses to applied stresses. They are so desirable for these types of studies as these types of flow chambers can use laminar flow to introduce shear stresses to endothall cells that will replicate the physiological microenvironment of the cells. As previously explored, is important to ensure that the laminar flow is full developed prior to reaching testing points, but parallel plate flow chambers allow for unique successful testing of endothelial cell's responses to different applied stresses [29]. An ideal feature of parallel plate flow chambers is that while they are commercially available, they are relatively simple to build and design for specific needs of the project. This allows for different flow paths, testing points, and applied shear stresses on the endothelial cells to be created specifically to meet the goals of a project [29].

An example from this study is that they required a parallel plate flow chamber that could be AFM-compatible for their analysis of their endothelial cells. For this uniquely designed flow

chamber the team of researchers used 316L stainless steel to create their plates as well as an O-ring to seal the chamber. Both materials were chosen with biocompatibility in mind in order not to harm the endothelial cells [29]. Once they had their endothelial cells and flow chamber assembled, they used a peristaltic pump connected to the inlet and outlet of the parallel plate flow chamber and this flow allowed shear stresses to be applied to the endothelial cells where they were exposed to a shear stress of 8 dyne/cm^2 for 15 hours. After 15 hours the cells were fixed with 4% paraformaldehyde and prepared for AFM measurements and imaging. This team reported that the parallel plate flow chambers allow for accurate exposure of endothelial cells to laminar fluid flow to study the biomechanical behavior of the endothelial cells [29].

3. Project Strategy

3.1 Initial Client Statement

The initial client statement was based on the unknown effect that pneumonectomies pose on the endothelial glycocalyx. It was to create a design for a flow device that allows for more accurate measurements of cellular changes under different conditions such as increased shear stress and fluid flow. This accuracy would allow for these changes to be studied in vitro to create a system to analyze how a change in fluid flow due to a pneumonectomy affects tissues in the body. The purpose of this project is to elucidate structural changes that occur to the pulmonary endothelial glycocalyx (an integral part of endothelial tissue contributing to flow regulation) due to increase in vascular flow after pneumonectomy using our device. These changes could be measured, and connections made from expression of specific endothelium regulating proteins changes under applied pneumonectomy flow conditions. Analysis of these components creates potential targets for future development in treatments for complications resulting from pneumonectomies.

3.2 Technical Design Requirements

3.2.1 Objectives

To meet the needs of the client statement the team identified the following objectives to help progress the project and meet the goals:

1. **Flow Simulations.** Develop computer models of the pulmonary arteries and run simulations to understand the blood flow patterns before and after a pneumonectomy. Then, use the data from the flow simulations to perform a statistical analysis to understand the significance of the change in shear stress.
2. **Design and Manufacture a Parallel Plate Flow Chamber.** A parallel plate flow chamber should be designed and developed to allow for in-vitro testing of endothelial cells. To stay within the budget of the project the material and manufacturer prices should only be a couple hundred dollars.

3. **In-Vitro Testing.** In-vitro testing utilizing human lung microvascular endothelial cells should be completed using a mechanical pump to introduce physiologically accurate flow to the cells. In-vitro testing should be done for both a control (normal scenario) and for left and right pneumonectomies to study the effects of shear stress on the cells under different conditions.
4. **Staining and Imaging.** Stain the HLMVECs from the in-vitro experiments with WGA and measure confluency and thickness to determine the magnitude of damage from different blood flows increasing the shear stress magnitude on the cells.

3.2.2 Constraints

There are multiple design constraints that need to be considered when planning the approach for this project. A primary constraint that posed a problem was the budget allowed for the project. The team had a total of $1,250 to meet all the listed objectives and design requirements. This was predicted to become a problem early on as the materials required for cell culture and staining of the cells were quite expensive, as were the additional materials needed to run the in-vitro testing (like the tubing required for the flow). Material price for manufacturing also had to be considered and this played a large part in the abandonment of fabricating a 3D model as the budget would not allow for the prototyping and fabrication of two separate models.

Other constraints that will be more defined in the following functional and specification sections include the capabilities of the device to meet the needs of the project (flow path design, adjusting for different experimental models, etc.), the overall size of the model for convenience, the biocompatibility, physiologically accuracy, as well as others which will be discussed in the following sections.

3.2.3 Functions

The 2D model must be designed as a functional flow chamber in order for flow simulation and in-vitro testing to be successfully completed. It must have a flow path that mimics the geometrical shape and features of the pulmonary arteries, and it must be able to be adapted to either be the control model (which is a no-pneumonectomy) or to be either a left or a right

pneumonectomy. It also must include entrance and exit points for the liquid and there must be a known input volume flow. This is required for both the flow simulations and the in-vitro experiments.

The 2D model must also have components that will allow for successful in-vitro flow experiments. This means that the flow chamber must be watertight, which can be completed by creating gaskets to prevent leaking. The flow chamber must also be able to incorporate HLMVECs where the cells can experience the flow without disrupting the flow. To do this the cells must have specific spaces where glass slides can be placed in the model. Ideally, cutouts in the flow path where glass slides can sit flush with the flow path. Lastly, the flow chamber needs to be biocompatible and must be made of materials that can be sterilized as cells will encounter the device.

3.2.4 Specifications

The design must meet specific requirements to perform for the experiments intended. The values for these requirements as well as functional and performance specifications can be found in *Table 1.* The model must be able to contain a flow rate that will correlate to a physiologically accurate amount of shear stress in the arteries. Based on values found in literature and calculations for the scale of our model, the normal flow rate in the pulmonary arteries was found to be 5 L/min [35], but due to the smaller size of the designed model this value would have to be scaled down to accurate shear stress can be applied to the flow path. This is the flow rate that would be applied to the cells and kept constant through all experimental models. The device also would need to be designed to prevent leaking and ensure that the flow is maintained and is laminar throughout the device. For the model we also wanted to make the flow chamber more representative of pneumonectomy conditions. This was achieved by blocking off flow to the chambers representing, for example, the right artery for a left pneumonectomy. The team decided to create models for a left and right pneumonectomy to compare to a control or no pneumonectomy model. Additionally, the flow to the arteries in the model would need to be cut off at a length comparable to where the arteries are cut in a pneumonectomy procedure. Based on values found in literature, this was determined to be at a length of 1-2 cm.

Additionally, the model must be representative of the physiological system, the pulmonary arteries. For this the diameters and angles of bifurcation of the arteries will be used to make the model anatomically accurate (these values are summarized in *Table 1)*. The flow chamber should be relatively small as it must be kept in an incubator while experiments are being performed to maintain cell viability. The model should allow for multiple points or indents within the chambers for slides seeded with cells. This will allow for the verification of cellular changes at different points within the arteries where differences in flow can be observed. The model will have to be biocompatible and not have an innate toxicity on the cells that will be used in the experiments. Leak and biocompatibility testing will be performed to ensure that the model meets these requirements. The cell type used in the model for our application would need to be representative of cellular changes that occur after a pneumonectomy. For this reason, we chose human lung microvascular endothelial cells (HLMVECs) that would reflect changes in increased applied shear stress and flow.

Table 1: Functions and specifications of the parallel plate flow chamber.

	Function	**Performance**
Model Type	• A model that allows for controlled flow, is biocompatible, and models arteries	• Glass slides: 10 mm x10 mm • Angles of Bifurcation: RPA-MPA= 125°, LPA-MPA= 112° [31] • Diameters: MPA= 29.5 mm, RPA= 19.8 mm, LPA= 22.1 mm [8] • Material: acrylic with Teflon gasket
Cell Type	• A cell type that models response to the change in flow and shear stress	• Human Lung Microvascular Endothelial Cells
Pneumonectomy	• Blood flow cut off to one pulmonary artery to model a pneumonectomy procedure	• Model Right, and Left pneumonectomy and Control/No pneumonectomy

		• The distance the artery will be cut is 1-2 cm
Blood Flow	• A constant blood flow (cardiac output) in all experimental models	• 5 L/min is average blood volume flow for the pulmonary arteries [38]
Shear Stress	• A pump to create controlled, laminar flow and shear stress on cells	• Cells on slide will be stained and imaged after experiments • The normal shear stress for the pulmonary arteries is approximately 5-20 dynes/cm^2 [39]

3.3 Engineering Standards

The main engineering requirement for a flow device is that the device be biocompatible and not affect the cells that are being exposed to the device. ISO 10993 is the standard that outlines this and explains the requirements a medical device must meet including hemocompatibility, reactivity, genotoxicity, carcinogenicity, and cytotoxicity. The most relevant being cytotoxicity, as the device is not interacting with blood components or a physiological environment; therefore, carcinogenicity and genotoxicity are not relevant. Cytotoxicity is reviewed in ISO 10993-5 and the requirements for testing are defined [30]. Cytotoxicity tests are considered screening assays used to evaluate living cells' reaction to the device in cell culture by testing cell viability or growth. Cytotoxicity tests assess cell death caused by a material by measuring the cell number before and after exposure to that material. As outlined in this standard, the device being tested is required to be sterilized before testing with a justifiable method to avoid microbial contamination of the cell culture. However, the methodology used to sterilize the device should not alter the properties of the material, thus affecting the viability of the results [30]. For the device created for this study, autoclaving and UV sterilization were used.

The standard outlines different test methods for use in analyzing the cytotoxic potential of the device. These include MTT assays, staining and observation of cell morphology, and bulk corrosion product analysis. These are performed using the cells of interest, or relevant to the

application of the device; in this case, HLMECs and culturing under standard conditions. The cells are then exposed to the device for the standard outlines; at minimum, 24 hours at 37°C [30]. After this time, the cell morphology can be assessed using SEM or the cells stained with MTT, DAPI or Trypan Blue to identify absorbance, nuclei, or cell death to correlate to the relative cell viability after exposure. The standard outlines that the results of the cell viability measurements after exposure to the material must meet approximately 80% confluency, if the viability is reduced to < 70%, that indicates that the material has cytotoxic potential [30]. The materials used for the device, acrylic, and Teflon, based on prior biocompatibility testing were ensured to have met the outlined requirements and not affect cell viability.

3.4 Revised Client Statement

After research, discussion, and defining of the objectives, functions, and specifications of the device needed, alterations were made to the initial problem statement to better suit the needs of the project. The revised client statement is as follows: Develop a parallel plate flow chamber that models the geometry of the pulmonary arteries including angles of bifurcation, diameters, and lengths to allow for more accurate measurement of cellular changes to the endothelial glycocalyx under pneumonectomy conditions such as increased shear stress and fluid flow.

The team's need statement, which was developed in parallel with the client statement is as follows: Pneumonectomies are common procedures that result in one of the patient's lungs being removed for various reasons including cancer or damage to the lung. Although it is a common procedure, the effects that a pneumonectomy procedure has on the vascular system are vastly understudied and could have unknown effects on the endothelial glycocalyx resulting in fatal post-procedure conditions. By creating a device that can replicate the effects of a pneumonectomy we hope to better understand how the pulmonary-vascular system is affected after this procedure in hopes of reducing the mortality rate and aid in future research and treatments.

3.5 Management Approach

The MQP would be completed throughout all four terms of the 2021-2022 Worcester Polytechnic Institute academic year. To complete all the goals that the team set out to achieve, specific plans were created for each month of the acidic year. Figure 3.1 is a broad Gantt chart of how the team planned out the school year. General tasks that the team wanted to complete were created and were assigned to certain months to finish the project in the brief time frame given.

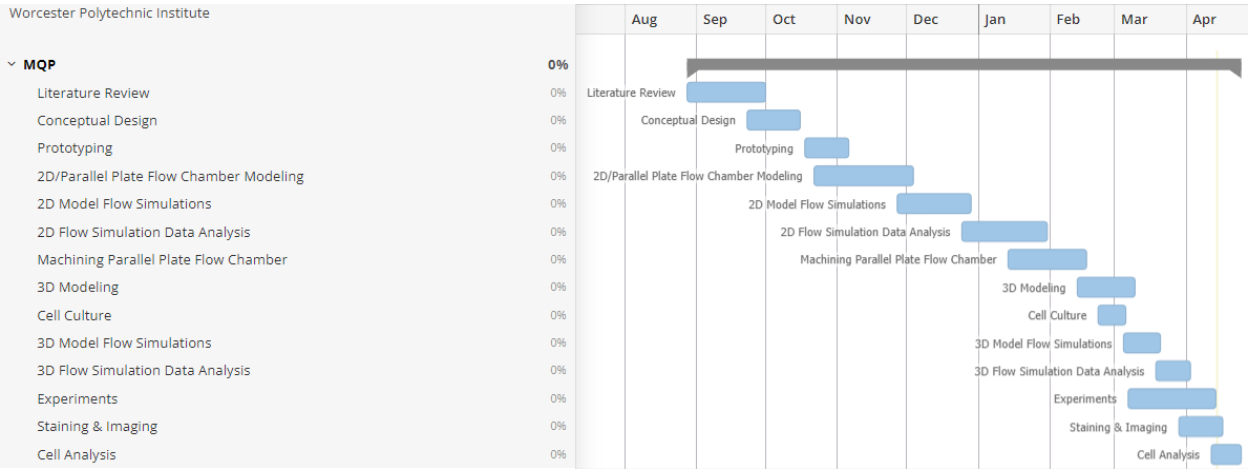

Fig. 3.1: Gantt chart for design process.

As seen in Fig. 3.1, the entire academic year, August through April, and the tasks performed each month are listed. In A Term, the team's goal was to perform a thorough literature review which would include cardio-pulmonary anatomy, physiology of the endothelial glycocalyx, pneumonectomy procedures, and similar studies. A term would end with conceptual designing of the in-vitro device that would be created for this project. B term, which started in October, began with prototyping the 2D model/parallel plate flow chamber which was created in Solidworks. Towards the end of the term flow simulations were also planned to be completed for this model. The plans for C term, which began mid-January, were to perform data analysis for the 2D flow simulations, machine the parallel plate flow chamber, begin the virtual 3D model, and begin the cell culture for upcoming experiments. Lastly, for D term, the virtual 3D would be finalized, and flow simulations and data analysis would be completed for that model. Also, in-vitro experiments, staining, imagining, and analysis of the endothelial cells would be completed by April when the project is due. It is also important to note that throughout the course of the year the MQP paper would be worked on as tasks were completed. April would mark the end of

the project and will require all the data analysis to be completed, the final report to be finished, as well as a professional presentation explaining the project.

4. Design Process

4.1 Needs Analysis

The design was created based on the need for a device that allows for more accurate measurements of cellular changes under different conditions such as increased shear stress and fluid flow. This accuracy would allow for these changes to be studied in vitro to create a system to analyze how a pneumonectomy, resulting in a change in fluid flow, affects glycocalyx layer. Gaining a better understanding of how the expression of specific endothelium regulating proteins changes under these conditions could allow for future development in treatments for complications resulting from pneumonectomies.

4.2 Design Requirements

The team originally set out to create both a 2D model and a 3D model. The 2D model became, more specifically, a parallel plate flow chamber based on the literature while the goal for the 3D model was to have it be as anatomically correct to the pulmonary arteries as possible. The following sections will go over the preliminary design choices for both the 2D & 3D model as well as go into design specifications for each model type. This will include design selection, conceptual designs, alternative designs, material needs, and fabrication needs.

For general requirements of the project the pulmonary artery flow path, the geometries for the pulmonary arteries were based on research and expertise from clinicians who perform cardiothoracic examinations or surgeries and their understanding of the geometry and function of the pulmonary arteries before and after a pneumonectomy. The angles of bifurcation for the pulmonary arteries are 112° for the MPA to the LPA and 125° for the MPA to the RPA [31]. The diameters of the main, left, and right pulmonary arteries respectively are 29.5 mm, 22.1 mm, 19.8 mm [8]. The system is scaled down by a factor of 0.75 within the device to replicate a realistic configuration while keeping the overall size of the parallel plate flow chamber relatively small. This allows for the measurement of cellular changes at specific points of interest in the chamber where there are known forces to be acting on the cells. These areas for optimal cell seeding in the design were determined based on fluid flow simulations where areas of shear

stress were significantly higher or lower to allow for variability between control and experimental samples.

Considering the model will be used to measure cellular changes based on fluid flow regulation, the material for the device must be biocompatible and not cause an explicit reaction from cells that could influence data collection. Additionally, the material had to be able to be machined to our specifications and prevent fluid from leaking within the structure. Both were accounted for when selecting the material.

The model had to be designed with indents in the bottom half of the chamber the size of a glass slide to allow for the slides, seeded with cells of interest, to be inserted and held in place. The indents were designed to be the depth of the glass slide to prevent the slides from disrupting the fluid flow in the chamber. The specific spots of placing the recesses for glass slides would be determined after completing flow simulations with flow path that mimics the pulmonary arteries.

The model is required additionally to allow for controlled and sustained laminar flow and minimizes disruptions that could influence data collection. The model will need to be able to be separated into two individual pieces to remove the glass slides after each experiment and still prevent the leaking of fluid from the separation between the pieces. The system must be closed so minimal air or other particles are able to enter. Therefore, the system must allow for a tight fit between connections to tubing for the microfluidic pump and the exit of fluid from the system. The system must also be able to have inlet and outlet holes to allow flow into and out of the system while using a mechanical pump.

Lastly, this model must be able to be manipulated to run all three experiment types that the team had planned: a no pneumonectomy, a left pneumonectomy, and a right pneumonectomy. Ideally it should be easy to manipulate the flow chamber to mimic a different condition and would not require a lot of additional material or time. To achieve both goals the team decided to create three different gaskets for three different experiment types. Gaskets are required to prevent leakage, but they can also be used to further control the shape of the flow path.

To begin designing, the team created a simple sketch of the pulmonary arteries, that included the important sections of the pulmonary arteries, a spot to start the flow at with a

mechanical pump, and where the desired place to cut off one of the arteries for a pneumonectomy would be. This preliminary sketch can be seen in Fig. 4.1.

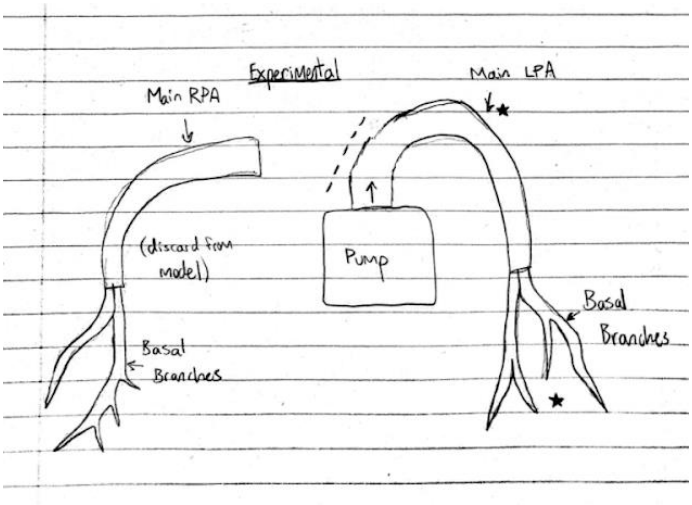

Fig. 4.1: Preliminary sketch of the pulmonary arteries with the desired arteries labeled, as well as the placement of inlet flow, and where the artery would be cut for a pneumonectomy.

After further discussion of the needs and goals of this project it was then decided to create a 2D version of the pulmonary arteries in the form of a simple flow path instead. The concepts in Fig. 4.1 were translated to a 2D style flow path well keeping the same concept. This newer design still takes into consideration the main sections of the arteries (but does exclude the basal branches), a spot to connect the mechanical pump for flow, and how to alter the model to mimic a pneumonectomy. These design changes were made with the need of in-vitro experiments in mind. These new design concepts can be seen in Fig. 4.2.

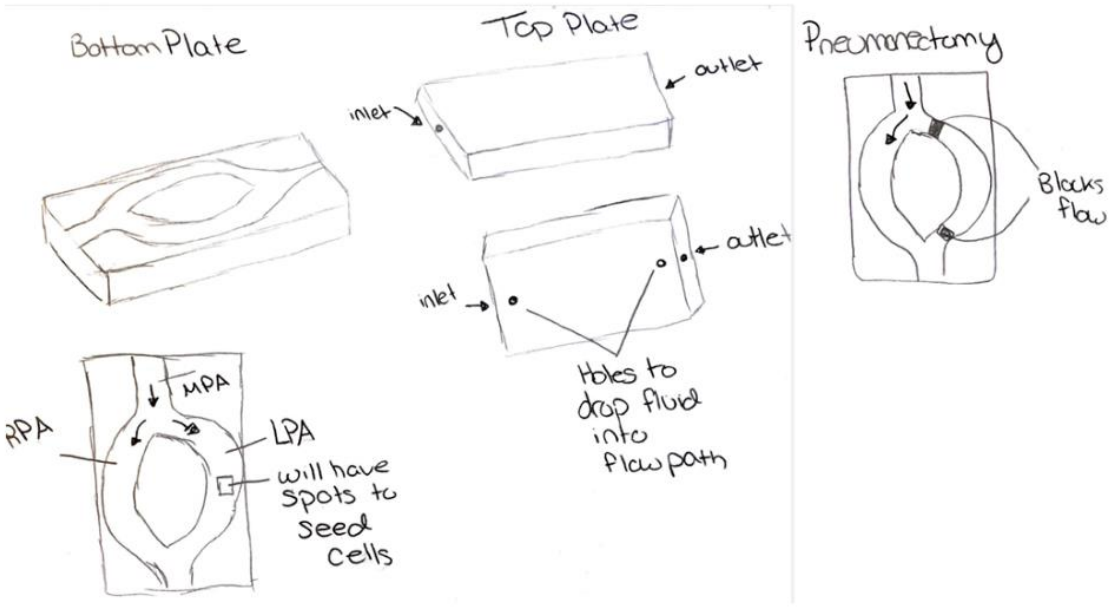

Fig. 4.2: Next stage in conceptual designing. This figure shows how the pulmonary arteries were created to be a simplified flow path. It also shows how flow would enter and exit the system via a top plate. Lastly it shows how a pneumonectomy would be modeled using this design.

After conceptually designing the model that would be used for this project, the team moved onto determining more specific features of the device. This included determining how to model and fabricate the design for virtual flow simulations and in-vitro testing.

4.2.1 Parallel Plate Flow Chamber Design Selection

It was determined that a parallel plate flow chamber would be the best approach to be able to mimic the flow that occurs in the pulmonary arteries and meet the needs of the 2D model. In general, parallel plate flow chambers allow for the application of well-defined and uniform shear stress to be applied to cultured cells [32]. A parallel plate flow chamber would also allow for the inclusion of glass slides with cells seeded to them for in-vitro experiments and cellular analysis. Three different parallel plate flow chambers that could meet our need were found throughout the literature and the three flow chamber designs that are being compared can be seen in Fig. 4.3 below.

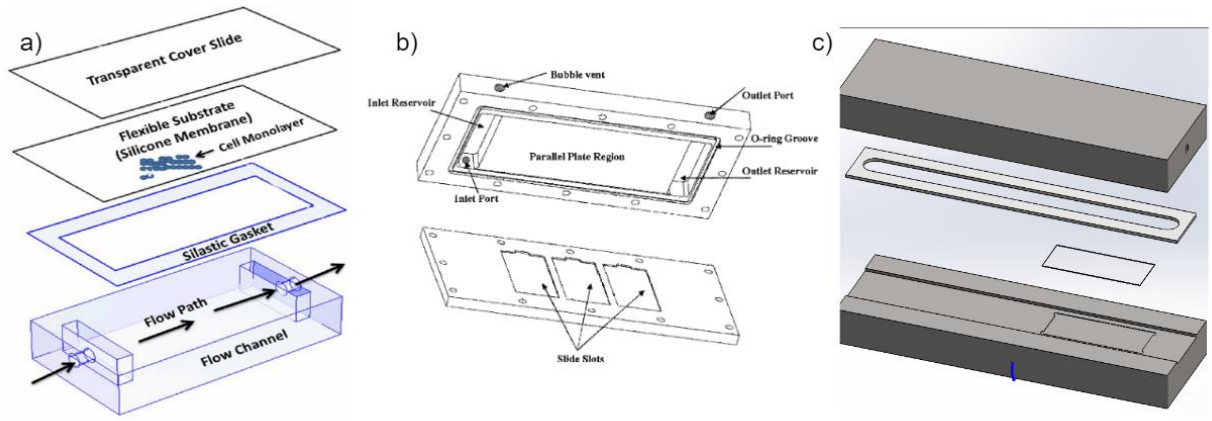

Fig. 4.3: Parallel plate flow chamber references. a) Design 1 from literature: Parallel plate flow chamber that uses a flexible substrate to seed cells to [27]. b) Design 2 from literature: Parallel plate flow chamber that includes multiple spots for seeding cells to [28]. c) Parallel plate flow chamber that is currently used in the Mensah lab at Worcester Polytechnic Institute.

The first design from Fig. 4.3 (a) has a simplistic design and uses a unique flexible substrate to place their cells. This design would be easy to assemble, but it would be difficult to use this model to create different flow paths. The goal of this project is to create a flow path that can mimic the shape of the pulmonary artery, and this design does not contain a flow path, thus the team would not be able to edit it for their needs. Another problem that arises with this device is that while the idea of a flexible substrate provides ease with seeding cells to it, it would be difficult to stay constant in ensuring that cells are seeded in the same specific place for every experiment [27].

The second design from Fig. 4.3 (b), while not intended for this use, was considered due to its multiple testing points. These testing points in this design were used to study when accurate shear stress values can be achieved in this type of parallel plate flow chamber [28]. For this project's need though, this idea of multiple testing points with multiple recesses for glass slides can allow for different testing points at different points of interest (possibly in the main pulmonary artery vs the left and right pulmonary arteries). This device poses a similar problem to the previous one, with this design it would be difficult to manipulate the flow path both to mimic the shape of the arteries as well as be able to be manipulated to run different experiments (control vs pneumonectomy experiment).

Lastly, is the flow chamber that is currently used in the Mensah lab at WPI which can be seen in Fig 4.3 (c). This flow chamber only has one spot to seed cells to, but the current design of the flow path could be easily manipulated to meet the needs of this project. This parallel plate flow chamber also uses a Teflon gasket which seems ideal for the unique shape of the flow path that this project would require.

4.2.2 Parallel Plate Flow Chamber Final Design Choices

A Pugh analysis was first completed comparing the three parallel plate flow chamber options seen in Fig. 4.3. The Pugh analysis ranked the three types of flow chambers on six different design aspects: affordability, functionality, leak prevention, multiple testing points, ease of machining, and the ability to manipulate the flow path. The Pugh analysis can be seen in Fig. 4.4.

Designs	Design From Literature #1	Design From Literature #2	Previously Used Model
Affordability	0	0	0
Functionality	0	0	0
Leak Prevention	1	1	1
Multiple Testing Points	0	1	-1
Ease of Machining	1	1	1
Ability to Manipulate Flow Path	-1	-1	1
Total Score	1	2	2

Fig. 4.4: Pugh analysis for comparing three different designs of parallel plate flow chambers. Ranking designs on their affordability, functionality, leak prevention, multiple testing points, ease of machining, and their ability to manipulate the flow path. Zero indicates an average score, a one indicates that this design excels at this feature, and a negative one indicates that this design cannot incorporate this feature.

The Pugh analysis determined that the first design from literature was not an ideal candidate for this project as it only scored a 1. As stated, this design lacked the ability to manipulate the flow path which is required for this project. Also, while it could have multiple testing points, the one big sheet of silicone substrate to seed cells too is not very ideal for

keeping the testing points consistent. The second design from literature scored a 2 on the Pugh analysis as it excelled in being able to have multiple testing points, but the design of the flow path reservoir in this design would prevent one from being able to manipulate the flow path which is required in this project to mimic the shape of the pulmonary arteries. The last design is the previously used model being used in the Mensah lab at Worcester Polytechnic Institute. This design also scored a 2 on the Pugh analysis as this was the one design that has an ideal base model to be able to manipulate the flow path, but unfortunately this model only has one testing point for cells.

Using the Pugh analysis, it was decided that the parallel plate flow chamber for this project would be a combination of the second and third designs. The second design is ideal as it allows for multiple slots for glass slides with cells and the third design has an ideal base model for being able to create multiple flow paths. Using these two designs the team worked towards creating a parallel plate flow chamber that would be able to mimic the shape of the pulmonary arteries as well as meet all the specified requirements.

4.2.3 3D Model Conceptual Design (Alternative Design)

As previously stated, the team had originally planned to make a 3D model as well for more anatomically accurate experiments, and while progress was completed, this ultimately became the alternative design. The goal for the 3D model was to be as anatomically correct to the pulmonary arteries as possible, specifically in the areas where the parallel plate flow chamber would be limited. This includes the accurate angles and diameters of the pulmonary arteries as previously stated for the 2D model, as well as the addition of the basal branches to the model. The basal branches, which are smaller segments of the pulmonary arteries, branch off the bottom of the main base of the left and right arteries. To make the 3D model more anatomically correct it was planned to incorporate the posterior basal segments off the right artery and the anterior basal segment and lateral basal segment off the left artery [4]. Adding these sections would allow for a deeper evaluation of the shear stress changes after a pneumonectomy in smaller sections of the arteries. Another feature of the 3D model will be that it will be cylindrical to match the shape of the pulmonary arteries more accurately. The parallel plate 2D model lacks the actual shape of

the arteries due to the nature of the device, so the 3D model will allow for more accuracy when it comes to the shape of the model.

Time constraints, as well as accessibility to materials and machinery, ultimately prevented the team from fabricating the entire model. While it may not have been fabricated for testing two large strides were completed for this model including an accurate Solidworks model for flow simulations and preliminary testing of materials and fabrication.

For the flow simulations, using known values from the literature as well as determining some values using 3D scans of the arteries and ImageJ an accurate shape of the pulmonary arteries would be created. The cardiac output can then be applied as the volume input flow and the shear stress can be measured throughout the model. For a pneumonectomy model, one of the arteries can simply just be detached in the Solidworks model and the flow simulations can be run again to see the changes in shear stress after a pneumonectomy. For prototyping, like stated this part of the project was abandoned in this stage to allow more time to work on the parallel plate flow chamber, but the team still studied ideas for the design. A negative mold of the arteries would ideally be created and using a liquid substance that could harden around the mold would be ideal to create this model. Considerations would have to be considered for the implementation of cells, possibly seeded to the material being modeled, as well as how to remove the cells for imaging. This poses questions about how to seed cells inside of the model once created, how to reseal the model after removing the cells (ensuring its watertight), and how to image the cells on the material they are seeded to.

4.3 Modeling

During this project two different models were designed using Solidworks. Firstly, the 2D model, which was based on parallel-plate flow chambers, that would be used for in-vitro experiments as well. The second design was a more anatomically correct 3D model, which was not planned to be physically fabricated. Both these models were designed using Solidworks and flow simulations were run with both models to collect preliminary data.

4.3.1 2D Model

As noted in the design specifications, the 2D model was designed as a flow chamber that would focus on data collection for the main pulmonary artery, the left pulmonary artery, and the right pulmonary artery. Specifically, the main area of study was at the bifurcation of the main pulmonary artery, where it splits into the left & right pulmonary arteries. The 2D model is a simplified version of the pulmonary arteries to collect preliminary data of the shear stress changes post-pneumonectomy. For the 2D flow chamber, the diameters and bifurcation angles are values based on the literature, but the flow chamber is not cylindrical, the entire length of the pulmonary arteries was not modeled, and other branching artery segments were not included. These more anatomically correct features will be addressed in the 3D model.

The 2D model was designed to be a parallel plate flow chamber which uses a mechanical pump to run flow through the flow chamber. The mechanical pump connects to the flow chamber at opposite ends via tubing for the flow to enter and exit the system. An inlet hole at the beginning of the chamber allows for flow that is being circulated by the pump to enter the flow chamber. The flow then runs through the indented paths in the model and is then expelled through tubing at an outlet hole at the opposite end of the flow chamber. This allows the pump to continuously run fluid through the model.

A preliminary bottom plate with a flow path was created to investigate the relative overall size of the model and to begin to learn how to create parallel plate flow chambers. Figure 4.5 shows some preliminary layouts that were designed using Solidworks. These preliminary models are early iterations of the bottom plate of the flow chamber. The bottom plate is a crucial part of the design as it includes the path that the fluid will run through as well as spaces to place glass slides seeded with HLMVEC.

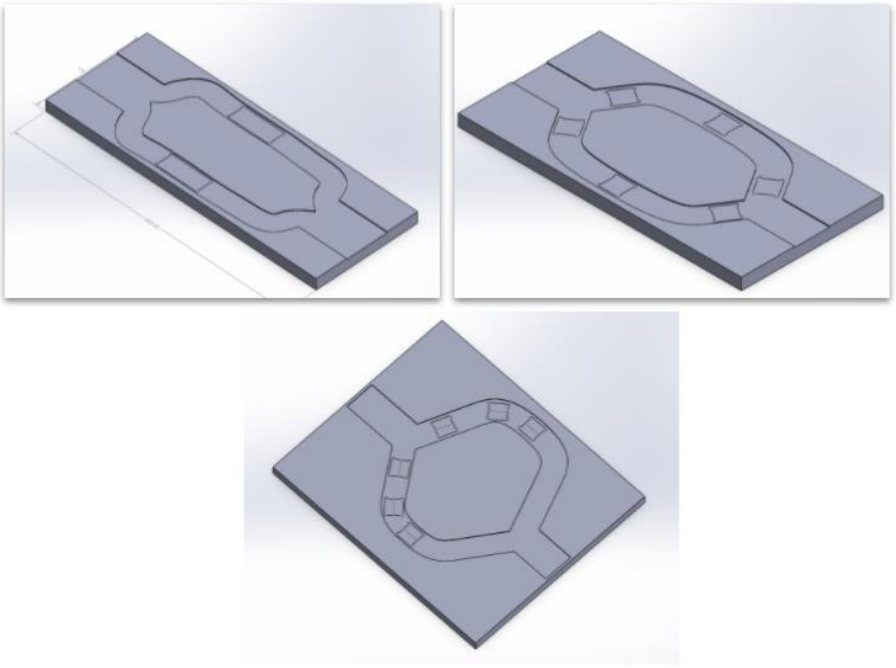

Fig 4.5: Preliminary designs for the flow chamber bottom plate.

With every iteration of Solidworks, the model became more detailed, more anatomically correct, and was adjusted to meet the team's needs. To make the model more anatomically correct, the diameters and bifurcation angles of the pulmonary arteries were used for the width of the chambers. To make the model a convenient size for testing all these dimensions were scaled down by 1:0.75.

The final aspect that was considered when designing the bottom plate was the location of spaces for the glass slides to sit during testing. The team wanted to place these in areas of highest expected changes in shear stress after pneumonectomy and used preliminary flow simulations to determine these points of interest. One glass slide was placed in the main pulmonary artery (after the flow has become laminar) to determine if there would be any change in shear stress in the main pulmonary artery after a pneumonectomy. The expected outcome was that the pneumonectomy would not affect the main pulmonary artery in terms of shear stress. Two glass slides each were also placed at the entrance of the left and right pulmonary arteries, directly after the bifurcation point. Finally, two more glass slides were placed farther down in each artery for a total of seven testing points in the 2D flow chamber.

After multiple iterations of designs, the final bottom plate of the flow chamber can be seen in Fig. 4.6. This figure shows a top view of the bottom plate of the flow chamber in Solidworks. The leftmost portion of the flow path mimics the main pulmonary artery and the right and left pulmonary arteries are modeled by the two parallel chambers that branch off the main artery with the left artery on top and the right artery on the bottom. The seven smaller indentations along the flow path were created to fit the glass slides. The glass slide spaces are 10 mm by 10 mm and have rounded edges to allow for the glass slides to be removed with tweezers after testing. The recess is only 0.15mm deep, to ensure that the glass slides sit flush with bottom of plate to not interrupt the flow. The plate itself is about 4 in wide by 7 in long and is 0.5 in thick. There are also twelve spaces for screw holes along the edges and in the center.

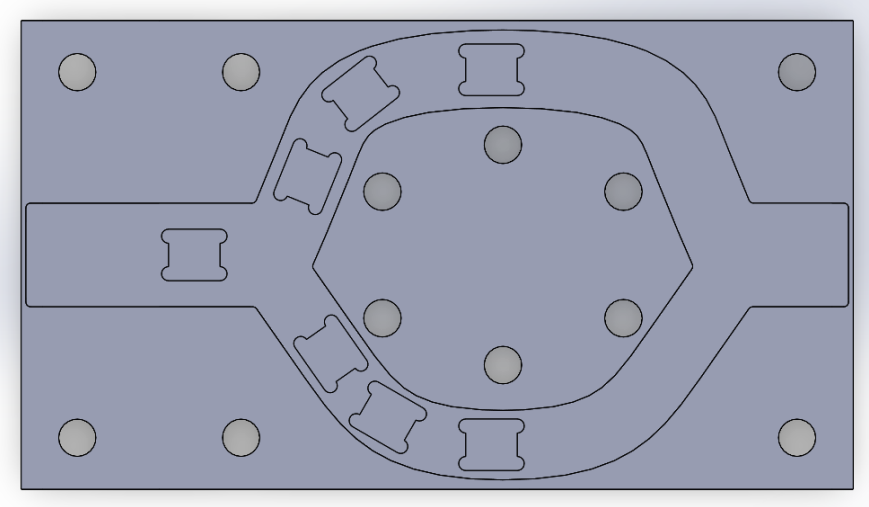

Fig. 4.6: Bottom Plate of 2D Flow Chamber Design

The other two components of the flow chamber that were designed and fabricated were the top plate and the gaskets. The top plate has two functions; allowing flow into and out of the flow path and to seal the flow path. The top plate was designed with the same screw holes as the bottom plate to secure the two together, as well as inlet and outlet holes to connect tubing. The inlet and outlet holes were centered on each end of the top plate and were tapped to allow a screw fitting to connect the top plate to the tubing. There are two small holes on the bottom of the top plate which are right below the inlet and outlet openings. These holes allow the fluid to drop down from the top plate into the flow path on the bottom plate and then be vacuumed up by

the tubing connected to the outlet hole. Images of the top plate created in Solidworks can be seen in Fig. 4.7**.**

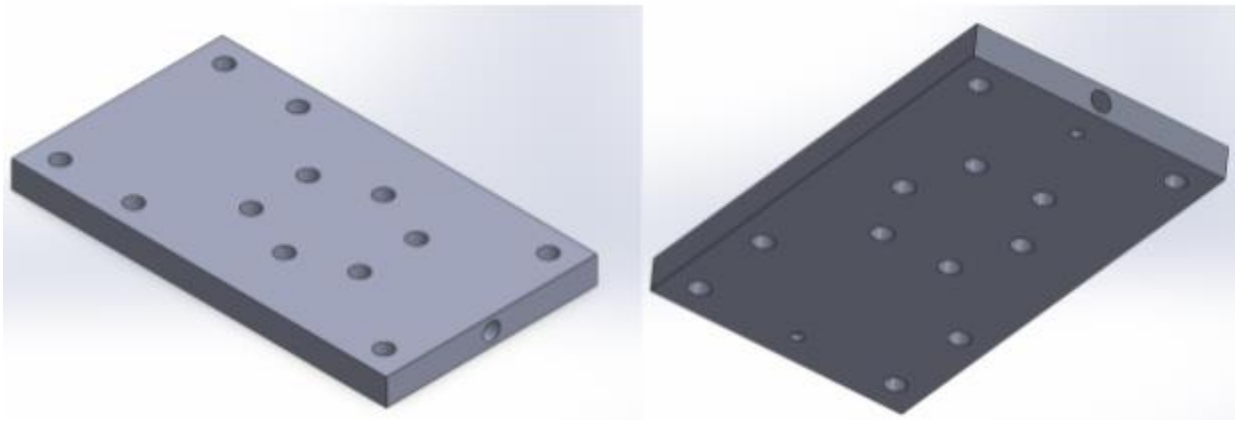

Fig. 4.7: Isometric view of Top Plate & View of the bottom/edge of the bottom plate.

The final piece of the assembly that was created was the gaskets. Gaskets allow the flow chamber to be watertight and prevent leaking. Three different gaskets were made for three different experiments. For the pneumonectomy experiments, the flow would have to be blocked off from entering either the left or right pulmonary artery. Instead of fabricating a separate piece to act as a blocker, gaskets that would block off the flow for the pneumonectomy models were designed. For the no-pneumonectomy model the gasket was the shape of the flow chamber and would sit inside of the flow chamber cutout. For the right pneumonectomy experiments, the right pulmonary artery was excluded from the gasket shape, while the left pulmonary artery was excluded from the gasket shape for the left pneumonectomy experiments. For both pneumonectomy type gaskets, the gasket blocks the flow 2 cm into the artery to mimic the amount of artery that remains after it is sealed off after a pneumonectomy. The three types of gaskets that were created in Solidworks for the flow chamber can be seen below in Fig. 4.8.

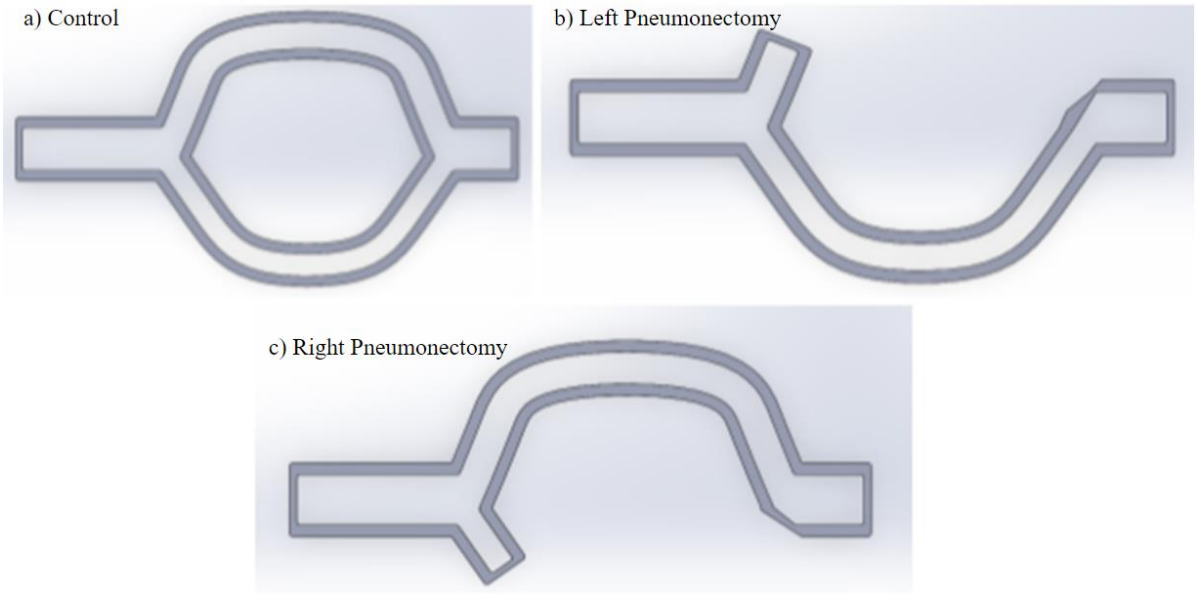

Fig. 4.8: Three different gaskets being used for three different experiments in Solidworks. a) Control “no pneumonectomy,” b) left pneumonectomy, c) right pneumonectomy.

For the final assembly, the bottom plate acted as the base, containing seven glass slides in the designated spaces. One of the gaskets was selected depending on the experiment type and was placed inside the cutout for the flow. The top plate was then placed on top of the bottom plate and gasket. The exploded view of the final assembly in Solidworks can be seen in Fig. 4.9.

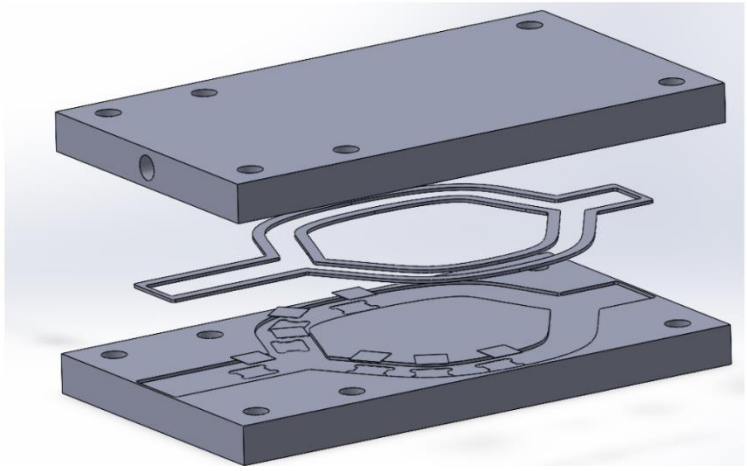

Fig. 4.9: Exploded view of full assembly in Solidworks.

4.3.2 3D Model

After the creation of the 2D model, design began for the virtual 3D model. This model was also created in Solidworks so similar flow simulations could be completed for both model types. The 3D model was intended to be a more anatomically accurate model of the pulmonary arteries. Unlike the 2D model, the modeled arteries of the 3D model were cylindrical and included more of the branching arteries off the left & right pulmonary arteries such as a few of the basal branches. Due to time limitations during this project, it was planned for the 3D model to be simplified by only including the pulmonary arteries and some of the basal segment, while any other arteries that segment off the main pulmonary arteries would be negated.

To understand the diameters, lengths, and branching angles of the basal segments to model them, ImageJ was used as there are very few mentions of these dimensions in current literature. An STL file of 3D reconstruction of a healthy patient's pulmonary arteries was used and imported into ImageJ [33]. To get the measurements for the basal segments' multiple different images of the STL file at different angles had to be used to collect all the measurements, but one of the images used can be seen in Fig. 4.10.

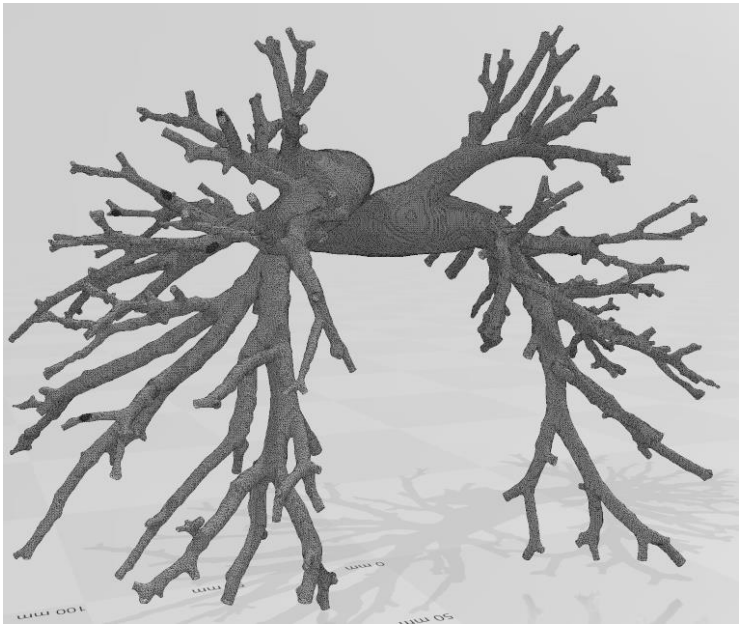

Fig. 4.10: STL of a medical image 3D reconstruction of a healthy human patient's pulmonary arteries [33].

The known diameters of the left and right pulmonary arteries, 22.1mm and 19.8 mm respectively, were used to set the scale in ImageJ [8]. Using this software, the values for the diameters, lengths, and branching angles for the pulmonary arteries and basal segments were collected and used to create the 3D model. While the figure above does show all the connective arteries, for the purpose of this 3D model they will mostly all be eliminated just leaving the left and right pulmonary arteries and the basal segments which are located at the end of the two main arteries.

To create the 3D model of the pulmonary arteries Solidworks was used again to create the main pulmonary arteries, the left & right pulmonary arteries, and the basal segments. A major difference between the parameters of 2D model design and the 3D model design is that the virtual 3D model was not created with the intent to manufacture for in vitro testing. For the 2D model, considerations had to be made about the entrance & exit of fluid through tubing as well as including specific sections to allow for the HLMVECs to be cultured. The 3D model was designed in Solidworks strictly for collecting virtual flow simulation data, so the previously listed considerations did not have to be met for the virtual 3D model. The 3D model which was created in Solidworks using values collected in ImageJ from analyzing 3D reconstructions of the pulmonary arteries can be seen in Fig. 4.11.

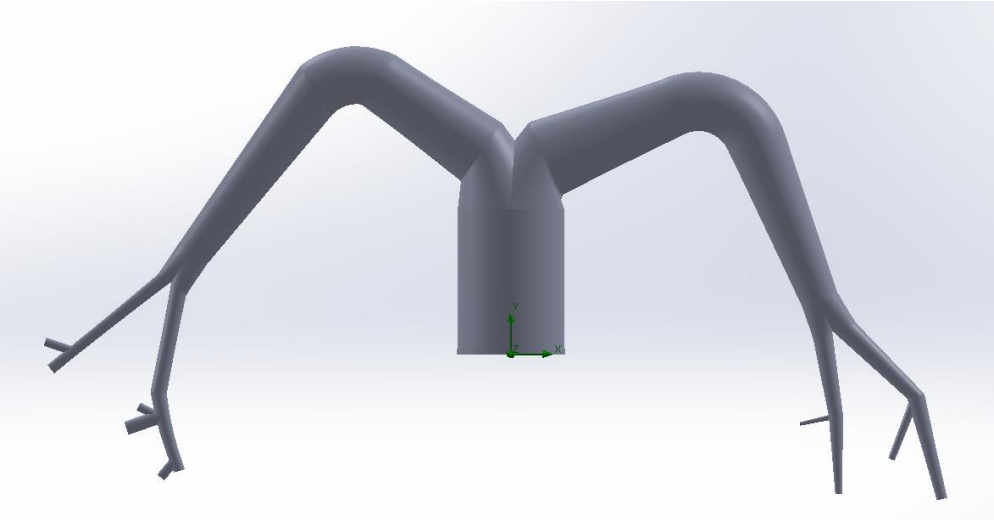

Fig. 4.11: 3D model of the pulmonary arteries with the basal segments created in Solidworks.

As stated, the 2D & 3D Solidworks models will both be used for flow simulations and the change in the shear stress due to a pneumonectomy on the artery walls will be analyzed.

4.4 Material Selection & Fabrication

Material selection was examined and studied for both model types, but the fabrication was only fully completed for the parallel plate flow chamber. While the 3D model did have some prototyping completed, a full model was not fabricated.

4.4.1 Material Selection for Parallel Plate Flow Chamber

Materials used for the 2D model needed to be biocompatible and meet design requirements. For seeding cells, 10x10 glass coverslips were used, as glass is typically used for cell culturing. The team debated between using acrylic and stainless steel for the top and bottom plates of the parallel plate flow chamber. Both are known for their biocompatibility, but ultimately the team chose acrylic due to its light weight, cheaper price, and the fact that it is clear, and the flow can be seen going through the model to ensure the flow chamber would be working as intended. UV-resistance acrylic from McMaster-Carr was bought and the specifications can be seen in Appendix A. Teflon (PTFE) was chosen for the gasket as previously used parallel plate flow chambers used by the team successfully use this material. Chemical-resistance Teflon PTFE from McMaster-Carr was purchased to create the three types of gaskets and the details can be found in Appendix A.

Additional materials include the 18-8 stainless steel screws that were selected to hold the bottom and top plate together as well as tubing to connect the flow chamber to the mechanical pump. Appendix A contains all the information and specifications for the final materials chosen for the model.

4.4.2 Fabrication Methods for Parallel Plate Flow Chamber

Prior to the fabrication of the parallel plate flow chamber the following materials were purchased: two 6” x 12” x ½” sheets of clear, scratch & UV-resistant cast acrylic and one 1/16” thick, 12” wide, and 12” long sheet of chemical-resistant slippery PTFE (Teflon). To begin the fabrication process, the Solidworks files were exported into ESPRIT. This was used for the

designation of the tools for creating the features on the parts, as well as the feeds and speeds of each tool. ESPRIT files were created for the top plate, bottom plate, and the three gaskets.

The acrylic plates for the top and bottom plates were cut to approximately the correct size using a laser cutter. The acrylic plates were then machined in the computer numerical control machine (VM2) in Washburn Shops at WPI. The tools used to machine the bottom plate were a CM 0.375-inch drill mill, a F drill, a ¼ inch end mill, and an ⅛ inch end mill. Three different orientations were required when machining the top plate to get the screw holes, the inlet hole, and the outlet hole. A CM .375-inch drill mill, a 3/16-inch drill, a ¼-inch end mill, and a ⅜-inch end mill were used to machine the screw holes in the first orientation. A CM .375-inch drill mill, a D drill, and a 1/16-inch drill were used to create the inlet and outlet holes in the other two orientations. Twelve 18-8 stainless steel pan head slotted screws (5/16: - 18 thread size, 1: long) were used to screw the top and bottom plate together.

A bandsaw was used to cut down the initial large sheets of Teflon into smaller pieces for each of the three gaskets. The Teflon itself was too thin to be placed into the machine and had to be secured to a sacrificial block of metal to machine. The smaller Teflon sheets were secured to the metal block using painters' tape and glue and machined in the VM2 using a 1/16-inch end mill to cut out the shape of the gaskets.

The machined flow chamber and the three gaskets can be seen in Fig. 4.12. The image on the left depicts the full assembly of the flow chamber with the "no-pneumonectomy gasket" in place. The image on the right depicts the three Teflon gaskets that were created for experimentation.

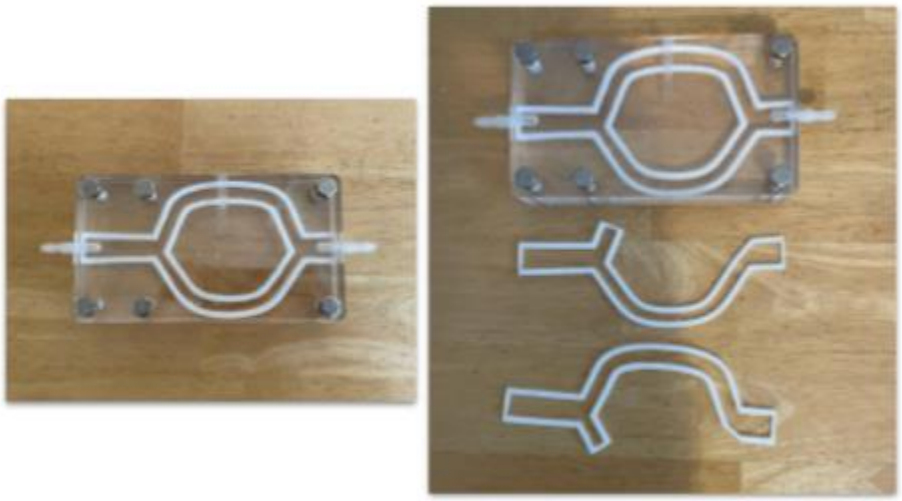

Fig. 4.12: Machined flow chamber. The image on the right shows the full assembly with the “no-pneumonectomy gasket” and the image on the left shows all three gaskets.

Edits to the design were made to incorporate more screw holes into the model after the initial fabrication. This created a more equal distribution of pressure throughout the model and provided more security to better hold the two plates together. The same tools used to machine the original screw holes were then used to add six more screw holes to the center area of the top and bottom plate. As seen in Fig. 4.13, the final model had a total of twelve screws.

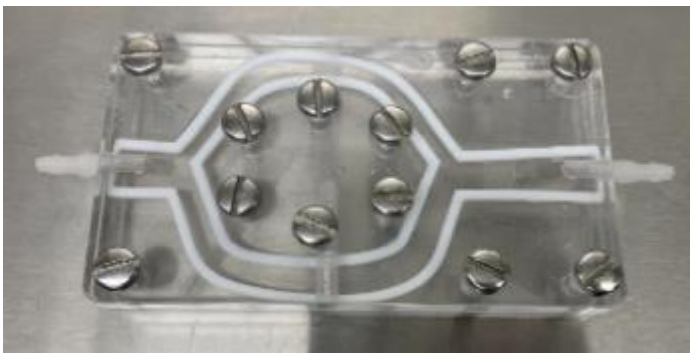

Fig. 4.13: Assembled parallel plate flow chamber with additional machined screw holes.

As designed, the flow chamber can be set up for three different experimental models, by using different gaskets. As previously shown, gaskets were created for the left pneumonectomy and right pneumonectomy model types and the incorporation of these gaskets into the model allows for either a left or a right pneumonectomy to be mimicked. The assembly for the left and right pneumonectomy flow chamber models can be seen below in Fig. 4.14. The process of

switching out the gaskets is simple as one only needs to unscrew and remove the screws, separate the two plates, take out the previous gasket, snap the desired gasket into place, and reassemble.

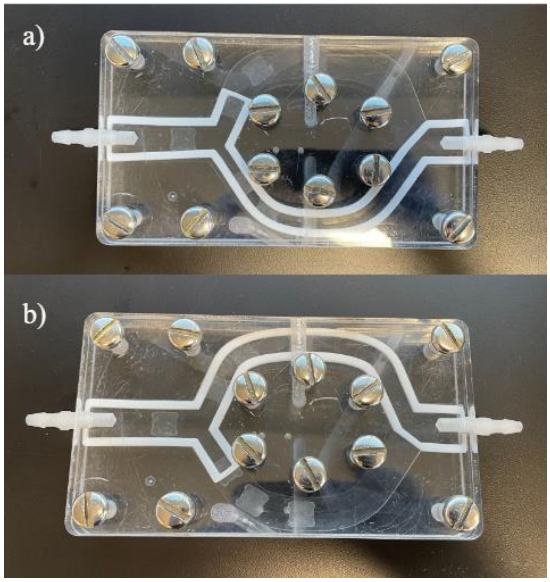

Fig. 4.14: Assembled parallel plate flow chamber for mimicking: a) a left pneumonectomy and b) a right pneumonectomy.

With the addition of Masterflex L/S® precision pump tubing, the Masterflex hose barb to thread adapters, 10mm by 10 mm glass slides, and the mechanical pump which were all either purchased or already available, the machined parallel plate flow chamber was ready for in vitro testing.

4.4.3 3D Model Materials & Fabrication

Like previously stated, the 3D virtual model of the pulmonary arteries was only created virtual flow simulations and the team had planned to fabricate the 3D model for in vitro testing by other means. For the 3D model, instead of seeding cells on glass slides, they would be seeded on PDMS tubes matching the configuration of the geometries of the pulmonary arteries. Different methods of fabricating such molds were explored; however, some devices that were examined early on, such as a bioprinter, were ultimately not available for the team to use, limiting the options determining the best way to create this element of the design. Based on prior research and recommendation it was determined that the best method was to use a mix-and-pour

style of PDMS, which would be purchased from Ellsworth Adhesives in a 0.5 kg kit [34]. To mold the PDMS, a negative of the model was necessary. A CAD model was created of a negative of a segment of the pulmonary arteries with dimensions selected from values the team had decided to use based on the literature. In Fig. 4.15, the first iteration of the CAD model is shown, with the outer tube and inner cylinder creating a thin gap for molding the PDMS. The negative mold would create a PDMS tube with the diameter of the inner cylinder and the wall thickness of the gap width. Although the first iteration of this mold was created in accordance with anatomical values, this meant that the wall thickness and gap for molding the PDMS was 0.11 mm [35], which was too narrow to properly pour the PDMS. Due to the shear stress measurements on the cells not requiring anatomical flexibility of the pulmonary arteries, the wall thickness was determined to be inconsequential if altered, and another iteration of the negative CAD model was created that used a wall thickness of 1 mm **(**Fig. 4.16**)**.

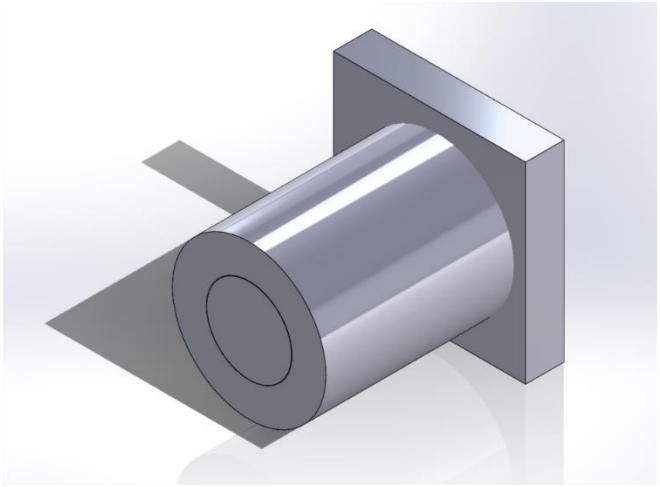

Fig. 4.15: First iteration of the negative mold for the PDMS tubes. The diameter of the molded PDMS tube would be 22.1 mm, and the wall thickness would be 0.11 mm, in accordance with anatomical values for the left pulmonary artery.

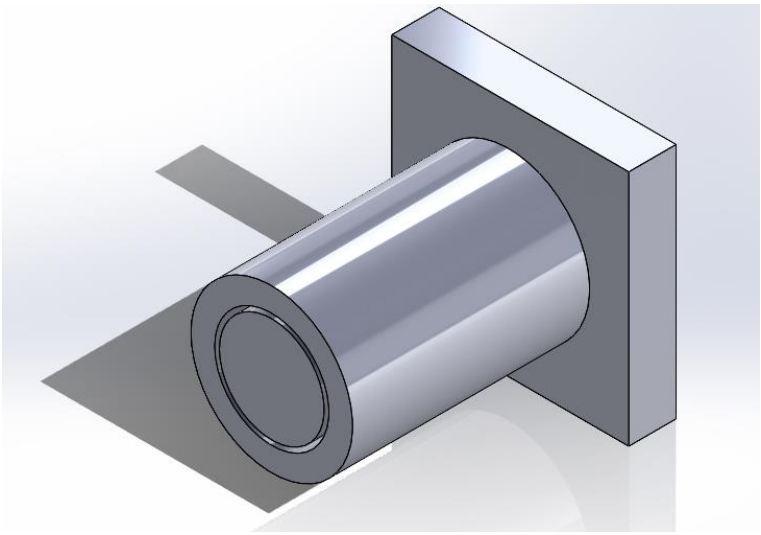

Fig. 4.16: Second iteration of the negative mold for the PDMS tubes. The diameter of the molded PDMS tube would be 22.1 mm and the wall thickness would be 1.0 mm to create a large enough gap to pour the PDMS into the mold.

The negative 3D print would be made using PVA filament, a sacrificial material that can be dissolved in water [36]. This helps to avoid issues with demolding, as the PDMS tube can demold itself if left in a water bath overnight. The PVA can also withstand the curing conditions of the PDMS, which is typically 60℃, and the final PDMS component washed with a mild detergent after demolding to remove any residue left by the PVA [37].

The 3D printed model was designed for each segment of the pulmonary arteries with the corresponding diameters. The mold was designed as one piece to avoid a seam in the PDMS created by multiple pieces being fitted together that could cause leaks or otherwise affect data collection. A smaller, straight tube was created as a means of testing the process, and more detailed models would have followed. Each model piece consisted of an outer tube with a solid cylinder in the center, creating the negative space of a tube in the desired diameter. These were attached to a flat base that extended a bit from all sides, making a stable surface that completely blocked off one end. To mold the PDMS, the negative was stood on its base and the PDMS was poured into it through the top. The negative was then dissolved in water, resulting in a PDMS tube that is open on both ends to allow the cells to be seeded on.

After reviewing the theoretical molding process and two negative mold test pieces that had been 3D printed, it was determined that the 0.11 mm gap would not work properly, and this

piece was discarded. Further testing and molding were completed with the 1.0 mm gap CAD model. For each iteration, the CAD model was sent to a high-resolution 3D printer and printed with PVA filament. After removal, the printed negative was washed with a mild detergent. The PDMS was then mixed as per the manufacturer's instructions, with a 10:1 (w/w) ratio of PDMS base to curing agent [34]. The mixture was stirred well to ensure full combining of the two parts, whereupon the PDMS mixture was poured into the PVA negative mold so that it is flush with the surface. The popsicle stick used for mixing the PDMS was used to scrape the PDMS on the surface of the mold back and forth until all the PDMS had entered through the gap. Excess PDMS was wiped off with a paper towel and discarded to prevent the end of the tube from becoming blocked off. The mold was then de-gassed in a vacuum chamber before being cured at a temperature of 60℃ for 4 hours to ensure complete solidification [37]. To demold, a water bath was created with room temperature deionized water and the entire mold was submerged in the water bath overnight [36]. When all the PVA from the negative mold was destroyed or at least detached from the PDMS tube, the PDMS tube was removed from the water bath and washed with a mild detergent to clean away any residue [37]. This method would have been employed to create more PDMS tubes and attach them together, possibly using a silicone sealant or plastic tubing connectors, to create an entire 3D model.

4.5 Experimentation

Once the parallel plate flow chamber was developed the team created a protocol for in-vitro testing. This involved the culturing of Human Lung Microvascular Endothelial Cells (HLMVEC), sterilization of the flow chamber, assembly of the in-vitro experiments, and running the experiments utilizing a mechanical pump.

4.5.1 Cell Culture

HLMVEC were cultured on glass coverslips and PDMS using microvascular endothelial cell growth media (sigma-Aldrich). The cells were seeded on either the 10x10mm glass slides or the PDMS and observed for 2 days to ensure confluence, incubated at 37 °C and 5% CO2. When cells were determined to be confluent, the glass slides were transferred to the flow chamber and

placed in the designated machined recess. This experiment required use of Experimental Media, which is a mixture of the microvascular endothelial cell growth media and bovine serum albumin, or BSA (Sigma-Aldrich). When assembled, the flow chamber was placed in the incubator, to ensure the cells were in a controlled environment with the same conditions they had while being cultured, with a temperature of 37 °C and 5% CO2. When the flow time was completed, HLMVEC were fixed with a quick wash of phosphate-buffered saline (PBS) and BSA solution, followed by a second solution of 2% paraformaldehyde and 0.1% glutaraldehyde in PBS for 30 minutes at room temperature. To label the glycocalyx, the cells were stained with wheat germ agglutinin (WGA; Vector Labs), for 2 days while being incubated at 4°C. Secondary detection will use a 1:1000 concentration of Alexa Fluor 488-conjugate, incubating for 30 min at 4°C. Followed by using DAPI, or 4′,6-diamidino-2-phenylindole, to stain the nuclei by mounting the samples onto VECTASHIELD antifade mounting medium (Vector Labs). The samples were sealed onto the glass slides using clear nail polish and were stored at 4°C while waiting to be imaged.

4.5.2 Experimental Sterilization

To prepare the top plate, bottom plate, and Teflon gaskets for use in the flow assay, they needed to be sterile. An autoclave was used to sterilize the Teflon, PDMS, and tubing. The autoclave kills microorganisms that may be present on the equipment by superheated steam. The acrylic was unable to be autoclaved, as the temperature required for the autoclave could damage the acrylic plates. Instead, ultraviolet (UV) sterilization was utilized. The plates were sprayed and wiped with 70% ethanol, and placed in the hood, under the UV light which disinfected the acrylic plates, the screws, and any other materials that were not able to be autoclaved.

4.5.3 Experimental Methodology

Experimentation can begin once the cells are confluent, and all components of the parallel plate flow chamber have been sterilized. Assembly of the flow chamber took place in a fume hood to keep all components sterile. The seven glass slides with the HLMVECs were placed in their designated spots in the bottom plate of the flow chamber. The Teflon gasket was

then placed around the outer edge of the flow path and was snapped into place. The top plate was then placed on top and screwed into the bottom plate. Tubing connectors were then screwed into the inlet and outlet holes in the top plate. Once assembled the flow chamber was moved into an incubator for a controlled environment of 37 °C and 5% CO2.

The controlled flow rate was set using a mechanical pump with cell culture media at 171.6 mL/min determined by previous research on flow rate. This was based on flow rates from literature in which the cardiac output in the pulmonary arteries was found to be about 5 liters/min [38], but the flow chamber path is smaller than the pulmonary arteries as the diameters were scaled down and the flow chamber is not cylindrical like the arteries. Based on the literature the average shear stress on the pulmonary artery walls is about 10 dyne/cm^2 [439], by using Solidworks flow simulations it was determined that a flow rate of 171.6 mL/min results in the anatomically correct shear stress values. Using the parallel plate flow chamber, the controlled flow rate was pumped through the flow chamber to test the effects of shear stress on the HLMVECs at the points of interest with glass slides.

Once placed in the incubator and hooked up to the tubing that connects to the mechanical pump the pump was turned on. At first the media slowly moves through the system and the flow rate is increased at a rate of 10 mL/min until the desired rate is reached to ensure no problems arise as the flow increases. The flow was run through the 2D model for each type of gasket simulating the paths for the control, right pneumonectomy, and left pneumonectomy models. In addition to the parallel plate flow chamber, the same type of cells was placed in the flow chamber as well. These cells were not subjected to any flow and acted as a control to ensure there were no previous problems with the cells prior to starting the experiment. For each experiment, the flow was run for 6 hours and afterwards the cells were fixed and stained. The cells were then imaged, and the thickness and confluency were measured and subsequently compared. The cells were then stained for heparan sulfate, claudin, and occluding tight junction proteins to measure the effects of shear stress on the components of the endothelial glycocalyx. Because these proteins and components affect the degradation of the endothelial glycocalyx, they will be able to determine the effects shear stress would have on this layer.

5. Final Design Verification

5.1 Flow Simulations

Flow simulations were completed on Solidworks for both the 2D and the virtual 3D model prior to manufacturing and performing the in-vitro experiments. First the flow simulations were completed on the bottom plate of the parallel plate flow chamber to determine points of interest where the team wanted to study the shear stress before and after a pneumonectomy. Then the shear stress magnitude at the glass slide positions in the flow chamber was calculated using flow simulations for all three experimental models (a no-pneumonectomy, a right pneumonectomy, and a left pneumonectomy) and the increase in shear stress due to a pneumonectomy can be calculated and compared between the models.

5.1.1 2D Model Flow Simulations

For the flow simulations of the parallel plate flow chamber an inlet boundary condition of 83.3 cm/sec^2 was applied to the inlet hole on the top plate and an outlet boundary condition of "total pressure" was applied to the outlet hold on the top plate. When activated, Solidworks has many different options to view the results of the flow simulations. The team primarily focused on data that related to the shear stress but was also curious about other factors such as the velocity and pressure of the flow. Figure 5.1 demonstrates the shear stress, velocity, and pressure overlays for the three experimental models (no-pneumonectomy, left pneumonectomy, and right

pneumonectomy).

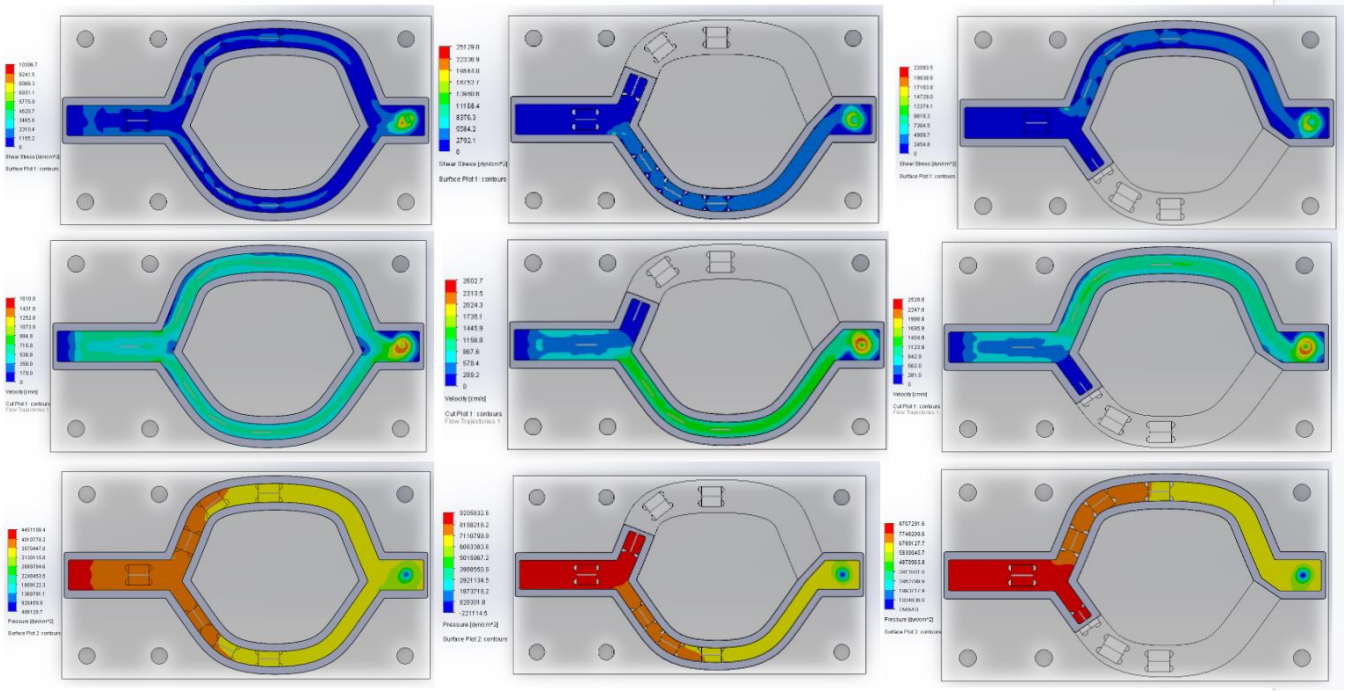

Fig 5.1: Flow simulation overlays from Solidworks. The first row is the shear stress overlay, the second row is the velocity overlay, and the third row is the pressure overlay. The first column is the no-pneumonectomy model, the second column is the left pneumonectomy model, and the third column is the right pneumonectomy model.

As stated, the team's main focus is the change in shear stress between the no-pneumonectomy model and the pneumonectomy models. As seen in Fig. 5.1, the first row demonstrates the difference in shear stress between all three model types. The no-pneumonectomy model overlay is mostly dark blue with small areas of light blue which means that there is little shear stress in the model. For the two pneumonectomy models, when one of the arteries was blocked off and all the flow was forced down only one artery, the shear stress in that remaining artery increased. This increase is noted by the lighter blue color being seen in almost the entirety of the remaining artery. While velocity and pressure were not the main focus, as seen in Fig. 5.1, like the shear stress, the velocity and pressure increase in the remaining artery after a pneumonectomy. The pressure also greatly increases in the main pulmonary artery section after a pneumonectomy as seen by the increase in red in the last row of Fig. 5.1 after a pneumonectomy.

To obtain numerical data about this change in shear stress, the seven testing points (which are defined by the indents for the glass slides with the cells to sit) were set to collect and create “XY plots” of the shear stress over the length of the glass slides. These testing points were all given unique names which can be seen in Fig. 5.2. These names will be used in all future data analyses for the 2D model.

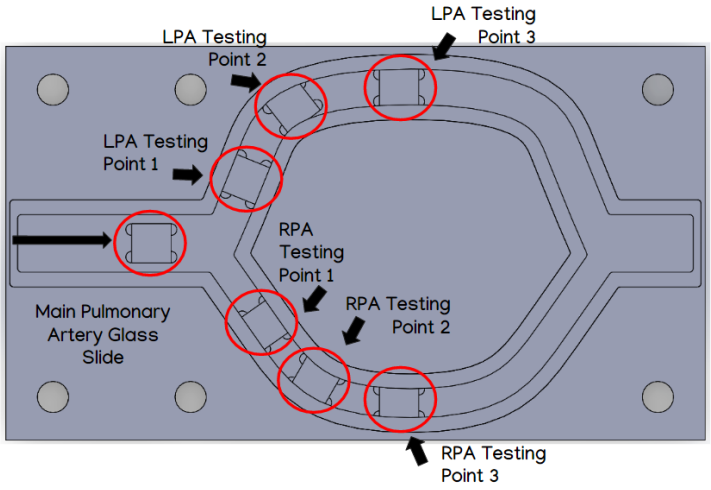

Fig. 5.2: Testing point locations & names for 2D model.

Three flow simulations were completed (one for each model type) and the shear stress values at each testing point were measured, collected, and exported in Excel. Instead of just being one data point the shear stress was measured at 0.2mm increments along the center of the glass slide. This resulted in 50 data points over the course of the 10mm glass slide for each testing point. This raw data was used to create the graphs seen in Fig.5.3. Figure 5.3 contains seven graphs, one for each testing point in the flow chamber. For each graph, the shear stress values found at the points of the glass slides were graphed, and the graphs contain data from each experiment type for easy comparison. In Fig. 5.3 the blue lines represent the control “no pneumonectomy model,” the red line represents the data from the left pneumonectomy, and the yellow line represents the data from the right pneumonectomy flow simulations.

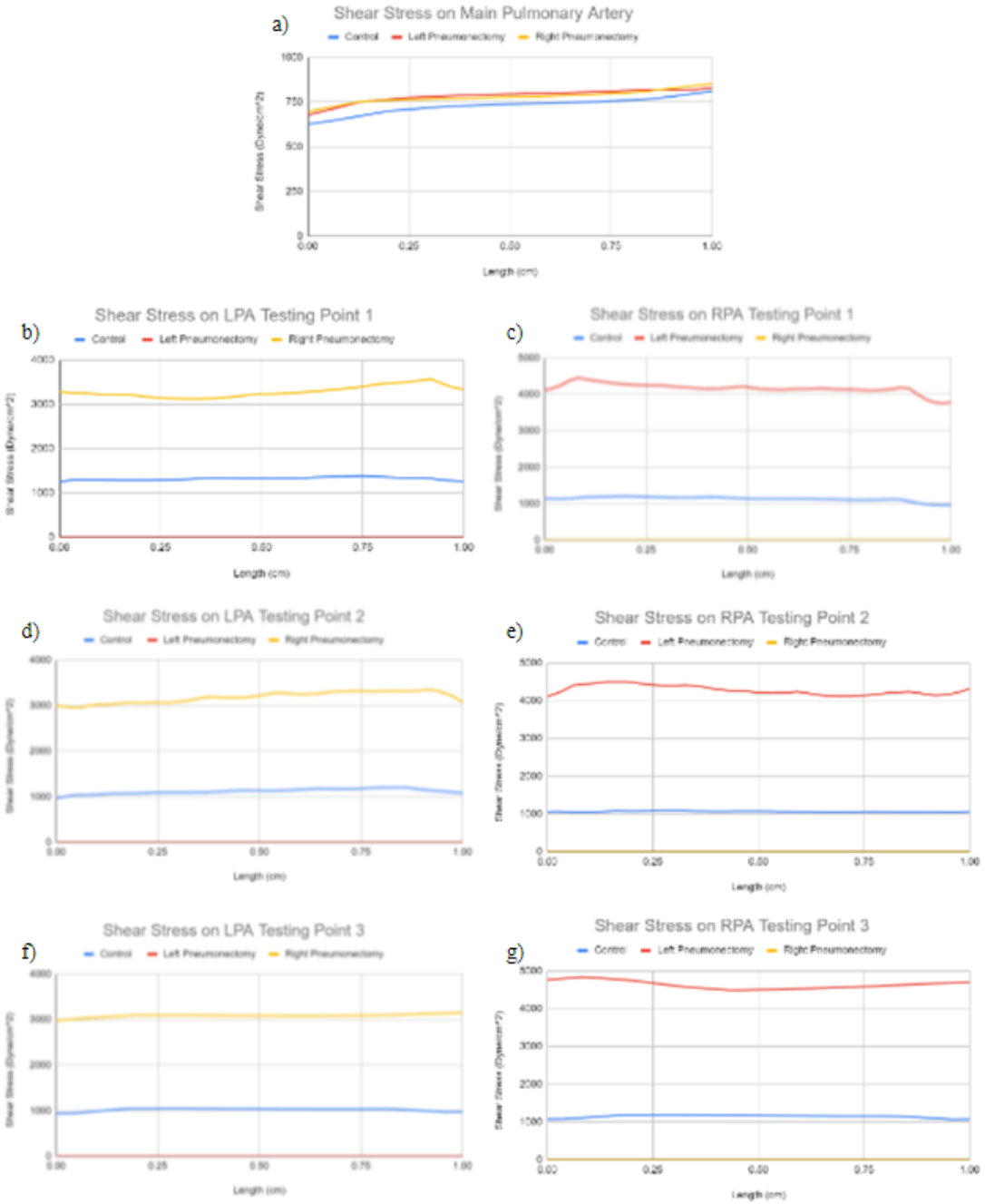

Fig 5.3: Graphs showing shear stress over the length of the testing points for all seven testing points during the three different experimental types. For all graphs, the blue, red, and yellow lines are the control, left pneumonectomy, and right pneumonectomy, respectively. a) MPA, b) LPA testing point 1, c) RPA testing point 1, d) LPA testing point 2, e) RPA testing point 2, f) LPA testing point 3, g) RPA testing point 3.

As seen in Fig.5.3, there is quite a significant increase in the shear stress between the no-pneumonectomy and the respective pneumonectomy models. First, as seen in part (a) of Fig. 5.3,

which compares all three experiments at the testing point in the main pulmonary artery, both the pneumonectomy models had a slightly higher shear stress when compared to the control, but the shear stress at this point for the two pneumonectomy models themselves were similar. For a right pneumonectomy, the increase in shear stress for the three LPA testing points was observed and the percent increase between the no-pneumonectomy model and the right pneumonectomy model was calculated. At LPA Testing Point 1 there was a 148.5% increase in the shear stress during a right pneumonectomy, at LPA Testing Point 2 there was a 184.5% increase in the shear stress, and for LPA Testing Point 3 there was a 201.9% increase in the shear stress. The same calculations were completed for the RPA Testing points as the shear stress increase was calculated between the no-pneumonectomy and the left pneumonectomy models. For this comparison, the increase in shear stress at RPA Testing Point 1 was 267.0%, at RPA Testing Point 2 the increase was 302.5%, and for RPA Testing Point 3 the increase was 303.3%.

Statistical analysis was completed using this data to determine if there was any significance for the increase in shear stress between the no-pneumonectomy and the pneumonectomy models. The graphs in Fig. 5.4 were created using GraphPad Prism, which demonstrates the shear stress fold change difference between the model types. The graphs also present the significant difference between the two treatments being compared, and the number of stars between the two treatments correlates to how significant the difference is. For the first graph, which was comparing all three models at the MPA Testing Point, an Anova analysis was completed to determine the significance. A T-test was used to determine the significance between the two treatments for the other six testing points. The final graph shown in that figure is an Anova analysis that compared all six testing points in the arteries to the testing point in the main pulmonary artery for the no-pneumonectomy model, which acts as the control.

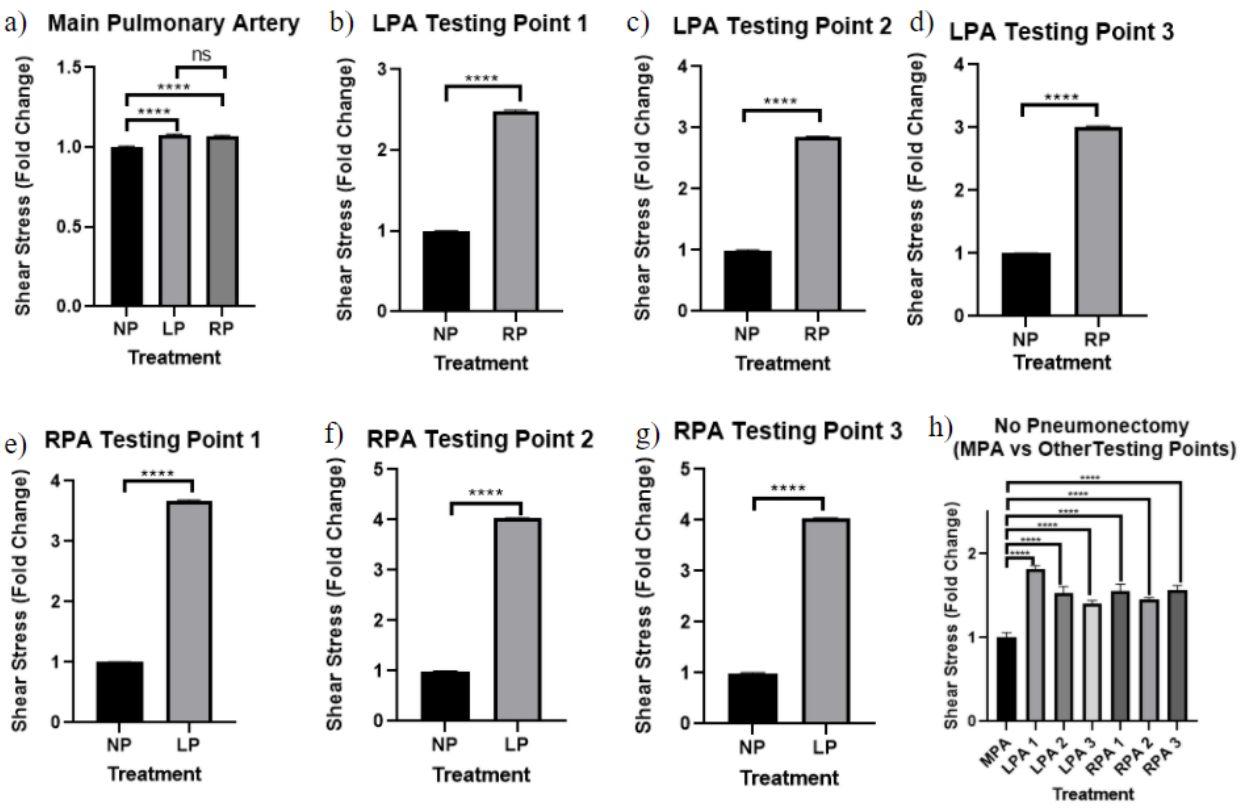

Fig. 5.4: Statistical analysis graphs that show the shear stress fold change difference between no-pneumonectomy and pneumonectomy models at the seven different testing points. The number of stars dictates how significant the difference between the different treatments is. A no-pneumonectomy model is denoted by (NP), a right pneumonectomy model is denoted by (RP), and a left pneumonectomy model is denoted by (LP).

As demonstrated by Fig. 5.4, the difference between the no-pneumonectomy model and the pneumonectomy models is significant. For the first graph, which was focused on the main pulmonary artery, there was a significant difference in the shear stress between the no-pneumonectomy and both the pneumonectomy models, but there was no significant difference between the right and left pneumonectomy models. There was large significance in the change in shear stress between the no-pneumonectomy model and the respective pneumonectomy model for the other six testing points. For a right pneumonectomy, there was an average of approximately a 3-fold increase in the shear stress at every testing point when compared with the no-pneumonectomy model. For a left pneumonectomy, there was an average of approximately 4-

fold increase in the shear stress at every testing point when compared with the no-pneumonectomy model.

The input volume flow for the 2D flow simulations was edited to determine an accurate flow for in-vitro experiments. While 5 L/min, which was used for the previous flow simulations, is physiologically accurate [38], for in-vitro experiments this was decreased to account for the smaller size of the model. The model is not cylindrical like the arteries and has a different volume than the actual pulmonary arteries, so to represent realistic shear stress observed on the arteries the volume input needs to be decreased. The shear stress in the pulmonary arteries for a healthy individual can range from 5-20 dyne/cm^2 according to the literature [39]. It was found that decreasing the inlet volume flow to 171.6 mL/min allows for shear stress values between 5.9 dyne/cm^2 to 17.7 dyne/cm^2, which is accurate for normal conditions of blood flowing through the pulmonary arteries. The shear stress overlay throughout the flow chamber for a no-pneumonectomy with the new inlet flow of 171.6 mL/min can be seen in Fig. 5.5.

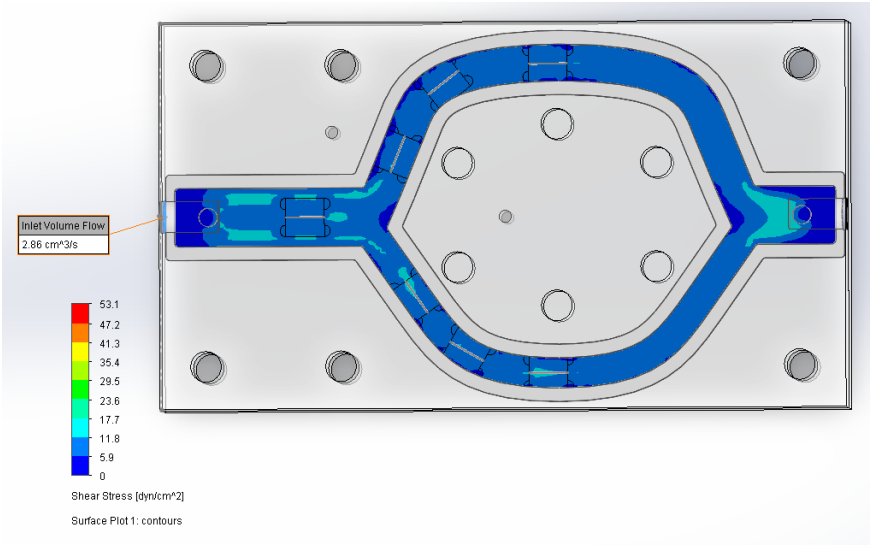

Fig. 5.5: Shear stress overlay from flow simulations in Solidworks for an inlet flow of 171.6 mL/min.

It should be noted that the shear stress values obtained in the previous flow simulations are much larger than the shear stress values obtained using the flow for in-vitro experiments. This is because the size of the model is smaller than the actual pulmonary arteries, to account for this the increase in shear stress after a pneumonectomy for this new volume output was

calculated. As only the volume input is being changed, the percent change between the control and pneumonectomy models should stay relatively the same.

After running the flow simulations with the updated input volume flow used for in vitro experiments, the expected shear stress values that should be observed in the in-vitro experiments were found. At the main pulmonary artery testing point: for the control, the shear stress is 11.27 dyne/cm^2, but after a right pneumonectomy this slightly increased to 11.68 dyne/cm^2 and after a left pneumonectomy it increased to 11.37 dyne/cm^2. The shear stress values in the left pulmonary artery for the control are 11.52 dyne/cm^2, 11.13 dyne/cm^2, and 11.55 dyne/cm^2 for LPA testing points 1, 2, and 3, respectively. When modeling a righty pneumonectomy, which forces all the flow through the left artery these values increase to 21.62 dyne/cm^2 for LPA testing point 1, 21.09 dyne/cm^2 for LPA testing point 2, and 20.66 dyne/cm^2 for LPA testing point 3. As for the right pulmonary artery, the average values seen in the control model are: 11.89 dyne/cm^2, 11.30 dyne/cm^2, and 12.09 dyne/cm^2 for RPA testing points 1, 2, and 3, respectively. When a left pneumonectomy is modeled and all the flow is forced through the right artery the shear stress at these points increases to 25.62 dyne/cm^2 at RPA testing point 1, 25.50 dyne/cm^2 at RPA testing point 2, and 26.58 dyne/cm^2 for RPA testing point 3. This virtual data will be used for future comparison between this data and the in-vitro cell analysis as this should be the actual shear stress magnitude applied to cells in the in-vitro experiments.

5.1.2 3D Model Flow Simulations

The flow simulations for the 3D model were a more accurate portrayal of the shear stress experienced in the pulmonary arteries. The 2D model simulations excelled in determining the percent increase in shear stress after a pneumonectomy, but the shear stress values themselves were not anatomically correct. The 3D model allows for more accurate findings of the specific shear stress values as well as the percent increase in shear stress after a pneumonectomy.

The 3D model can be broken into 26 different sections, which means that the shear stress can be measured separately for each section. The breakdown of the different sections can be seen in Fig. 5.6. As seen in the Fig. 5.6, the main pulmonary artery is one large section, as this area is primarily a straight cylindrical section of artery. The left and right pulmonary arteries consist of

four sections each. The first sections are the beginnings of the arteries, directly after they branch off the main pulmonary artery at the bifurcation point. Then, the arteries continue into a longer straight second section, a third section where the arteries curve downwards, and a fourth section which is a long section of artery located in the lung where smaller segments (such as the basal segments) begin. The basal segments are split into four different categories depending on their location. The left and right pulmonary artery each have two different branches of basal segments and those segments have their own additional branching segments. As seen in Fig. 5.6, the two basal segments of the right pulmonary artery are referred to as B-S 1 and B-S 2, and the two basal segments of the left pulmonary artery are referred to as B-S 3, and B-S 4. The first basal segment grouping has three components, the second basal segment grouping has six components, the third basal segment grouping has four components, and the fourth basal segment grouping has four components.

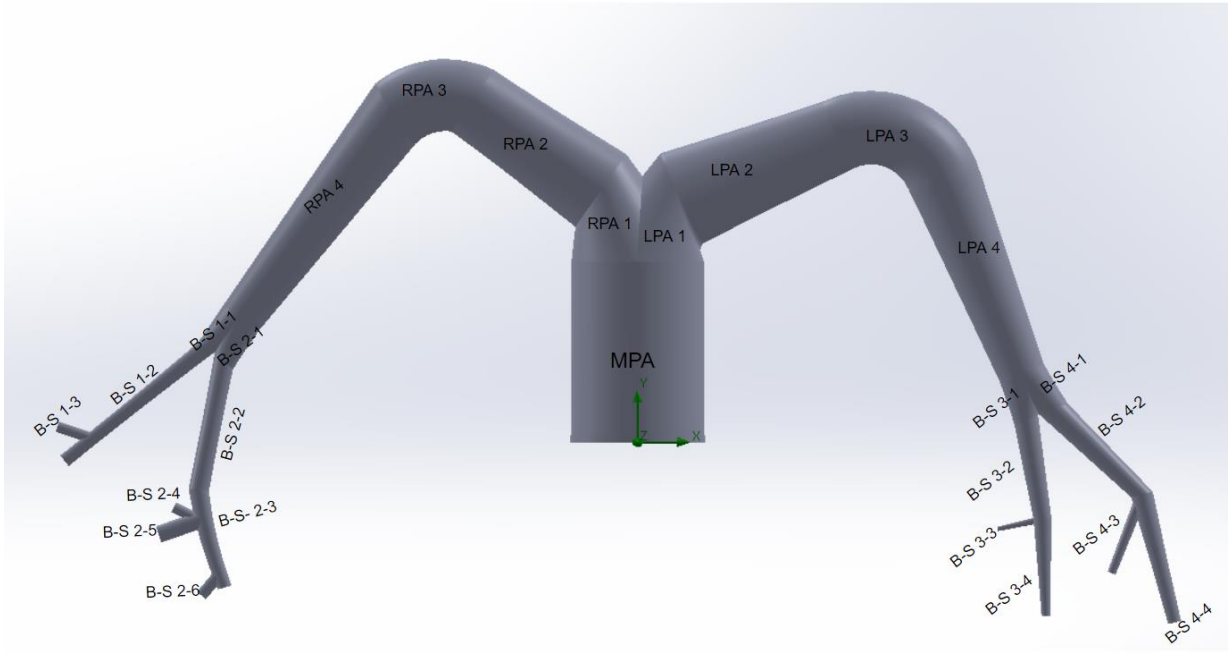

Fig. 5.6: Diagram of 3D Solidworks model with labels. The two basal segments of the right pulmonary artery are referred to as B-S 1 and B-S 2, and the two basal segments of the left pulmonary artery are referred to as B-S 3, and B-S 4.

Flow simulations similar to those completed for the 2D model were completed for the 3D model as well, using the 3D model that was created using Solidworks. The volume flow was introduced at the main pulmonary artery and was set to be 5 L/min (83.3 cm/sec^2). The outlet

boundary condition was set at all the open ends of the basal segments to “total pressure.” Unlike the 2D model, the 3D model is an accurate representation of the pulmonary arteries, as the diameters, lengths, and branching angles are anatomically correct. The input volume flow was physiologically accurate (5 L/min) and resulted in accurate shear stress values in the pulmonary arteries.

Similar to the 2D model, Fig. 5.7 was created for the 3D model which demonstrates the overlay of the shear stress, velocity, and pressure for each model type. The main change in the overlays is seen at the basal branches, especially in the cases of the shear stress and pressure overlays.

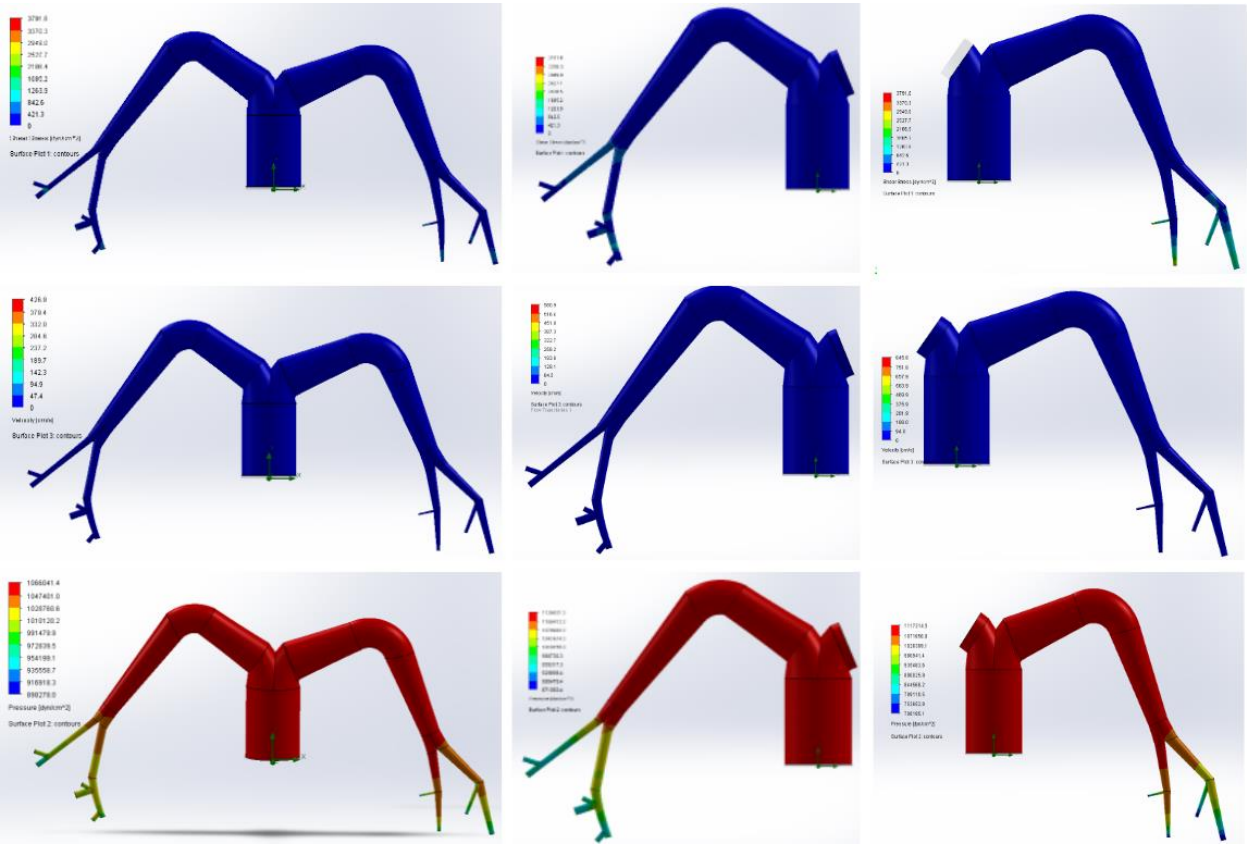

Fig. 5.7: Flow simulation overlays for 3D models made in Solidworks. The first row is the shear stress overlay, the second row is the velocity overlay, and the third row is the pressure overlay. The first column is the no-pneumonectomy model, the second column is the left pneumonectomy model, and the third column is the right pneumonectomy model.

The larger sections of arteries in the overlays presented in the figure do not demonstrate a visible change in the shear stress after a pneumonectomy as there is no change in the color. However, quantitative analysis does demonstrate that there are changes in the shear stress at these points after a pneumonectomy. The lack of change of color in the larger sections of the arteries is due to the significant increase in the shear stress, velocity, and pressure and the basal segments. As seen in Fig. 5.7, the basal segments do experience a visual increase in the shear stress and pressure large enough to cause significant color changes. This was expected and was the reason the team felt the need to include the basal branches in the 3D model.

Figure 5.8 shows the change in the magnitude of shear stress in the main pulmonary artery. There will always be blood flow in the main pulmonary artery for these three experimental model types, as the flow is not physically affected by a pneumonectomy. The shear stress data was collected at the main pulmonary artery for all three model types, which allowed for an Anova analysis to be used to compare the shear stress fold change between the three models.

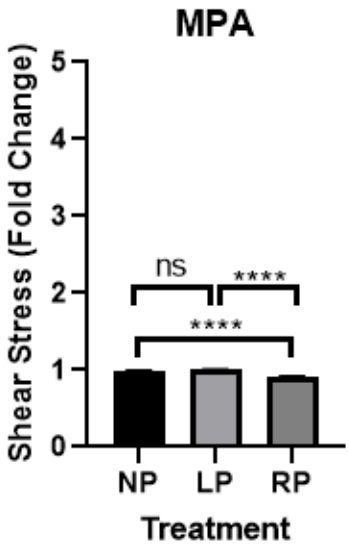

Fig. 5.8: Anova analysis for shear stress change in the main pulmonary artery.

The Anova analysis demonstrates that there is no significance between the no-pneumonectomy model and the left pneumonectomy model, but it does present that there is significance between the no-pneumonectomy model and the right pneumonectomy model, as

well as between the two pneumonectomy model types. There was an average shear stress of 1.68 dyne/cm^2 for the no-pneumonectomy model, an average shear stress of 1.70 dyne/cm^2 for a left pneumonectomy model, and an average shear stress of 1.56 dyne/cm^2 for a right pneumonectomy model.

The other two segment analyses that utilized Anova analysis were the RPA 1 and LPA 1 segments. After a pneumonectomy, a portion of the artery being removed is left behind, which means that blood is still able to flow through this portion of the artery before it is blocked by the sealed artery. This means that the blood is still allowed to flow through this 2 cm portion of the removed artery. Figure 5.9 is the Anova analysis for segments RPA 1 and LPA 1.

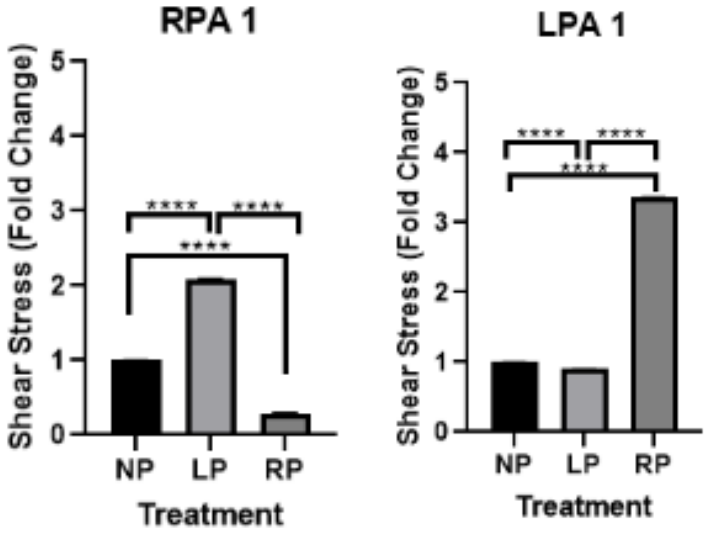

Fig. 5.9: Anova analysis for RPA 1 and LPA 1 segments.

As seen in Fig. 5.9, the shear stress increases significantly in the remaining pulmonary artery after a pneumonectomy. For a left pneumonectomy, the shear stress in the first section of the right pulmonary artery increases from 4.98 dyne/cm^2 to 10.44 dyne/cm^2 and for a right pneumonectomy, the shear stress in the first section of the left pulmonary artery increases from 2.25 dyne/cm^2 to 7.56 dyne/cm^2. The shear stress magnitude decreases after a pneumonectomy for the remaining section of the removed pulmonary artery. There is a significant decrease in the RPA segment 1 after a right pneumonectomy as the value decreases from 4.98 dyne/cm^2 to only 1.49 dyne/cm^2. While still significant, there is a smaller decrease in shear stress in the LPA segment 1 after a left pneumonectomy, from 2.25 dyne/cm^2 to 2.05 dyne/cm^2. The shear stress

magnitude in the 2 cm remaining section of the removed artery is smaller for both pneumonectomy model types but this decrease is more prevalent in the right pulmonary artery segment 1 after a right pneumonectomy.

T-tests were used for the remaining data analysis, as only two models are being compared, either a no-pneumonectomy and a left pneumonectomy, or a no-pneumonectomy and a right pneumonectomy. First, Fig. 5.10 presents the three remaining sections of the right pulmonary artery. For each of these three segments, the shear stress fold change between a no-pneumonectomy and a left pneumonectomy were compared using a T-test analysis.

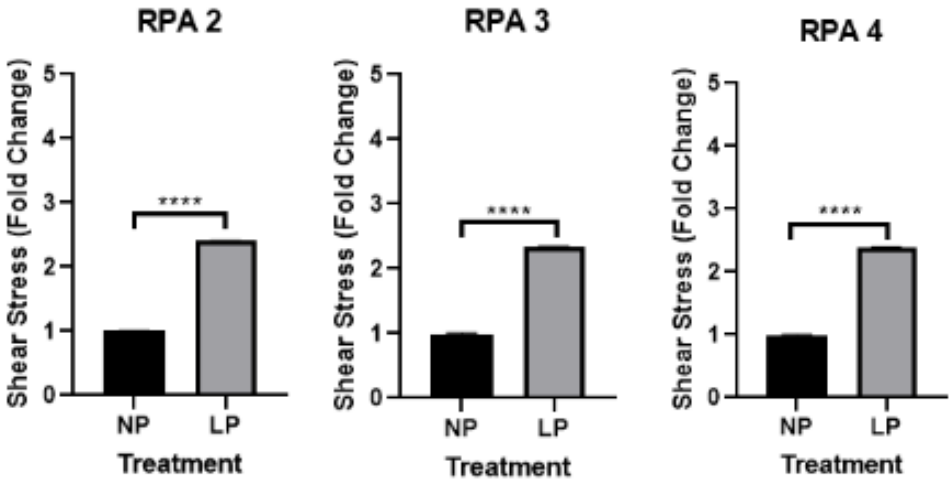

Fig. 5.10: T-test analysis for the right pulmonary artery segments after comparing shear stress fold change between a no-pneumonectomy and a left pneumonectomy.

As seen in Fig. 5.10, each section of the right pulmonary artery has approximately a two and a half shear stress fold increase after a left pneumonectomy. For all three of these segments, this increase in shear stress fold change due to pneumonectomy is significant. In the RPA segment 2, the normal shear stress experienced in the no-pneumonectomy model is 3.98 dyne/cm^2, and after a left pneumonectomy the shear stress in this segment of the artery increases to 9.57 dyne/cm^2. For segment 3 of the right pulmonary artery, which contains the major curve of the artery, the average shear stress pre-pneumonectomy is 4.02 dyne/cm^2, but after a left pneumonectomy the shear stress increases to 9.39 dyne/cm^2. For segment 4, which is the longest segment of the RPA, the initial shear stress before a pneumonectomy is 14.68 dyne/cm^2 and after a left pneumonectomy, the shear stress increases to 35.18 dyne/cm^2.

The next set of T-tests were completed for the first grouping of basal segments. This first grouping of basal segments branches off the right pulmonary artery and was broken into three different sections for analysis. The T-test analysis of the shear stress fold change between the no-pneumonectomy and the left pneumonectomy models can be seen in Fig. 5.11**.**

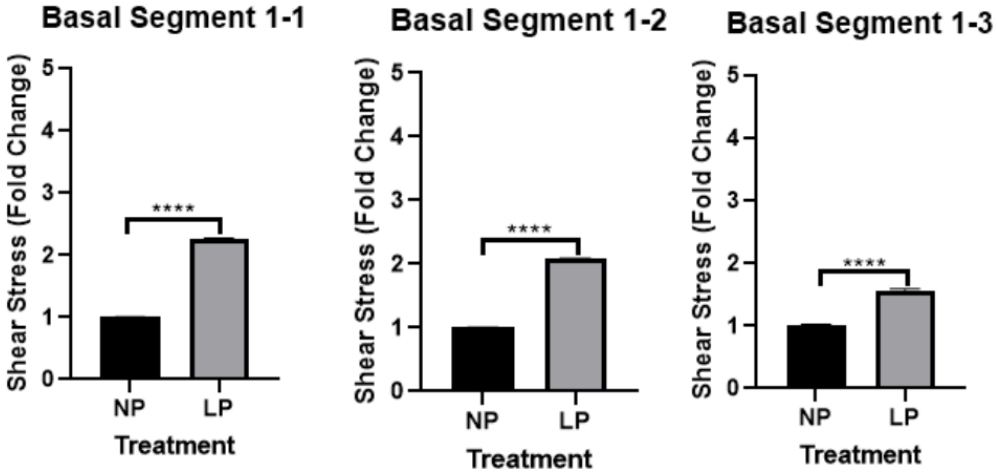

Fig. 5.11: T-test analysis for the first set of basal segments after comparing shear stress fold change between a no pneumonectomy and a left pneumonectomy.

The basal segments experience an increase in the shear stress as the basal segments are a smaller portion of the pulmonary arteries. This smaller size results in the wall shear stress increasing as the size decreases. As seen in Fig. 5.11, the shear stress in these three basal segments, on average, doubles after a left pneumonectomy. The average shear stress in basal segment 1-1 is 125.71 dyne/cm^2, and a left pneumonectomy causes the shear stress experienced by this segment of the basal branch to increase to 284.81 dyne/cm^2. The average shear stress observed in basal branch segment 1-2 is much higher, at 268.42 dyne/cm^2, and after a left pneumonectomy the average shear stress experienced at this segment increases to 557.01 dyne/cm^2. The average shear stress experienced before a pneumonectomy by basal branch segment 1-3 is 131.37 dyne/cm^2, and after a left pneumonectomy the shear stress increases to 205.97 dyne/cm^2. The different segments of the basal branches vary in diameter, length, and branching angle, which plays a significant role in their experienced shear stress. Since the basal segments all have unique dimensions, the shear stress varies significantly between them, which is observed in the previous values. Even if the basal branch segments all experience different

shear stress for the no-pneumonectomy model, all the basal segments experience a significant change in the shear stress fold change after a pneumonectomy.

The second grouping of basal branch segments are also part of the right pulmonary artery. This grouping was broken into six different segments and a T-test analysis was completed for each segment comparing the shear stress fold change increase between the no-pneumonectomy model and the left pneumonectomy model. Fig. 5.12 displays the T-test analysis for the six different basal branch segments in the second grouping of basal branches.

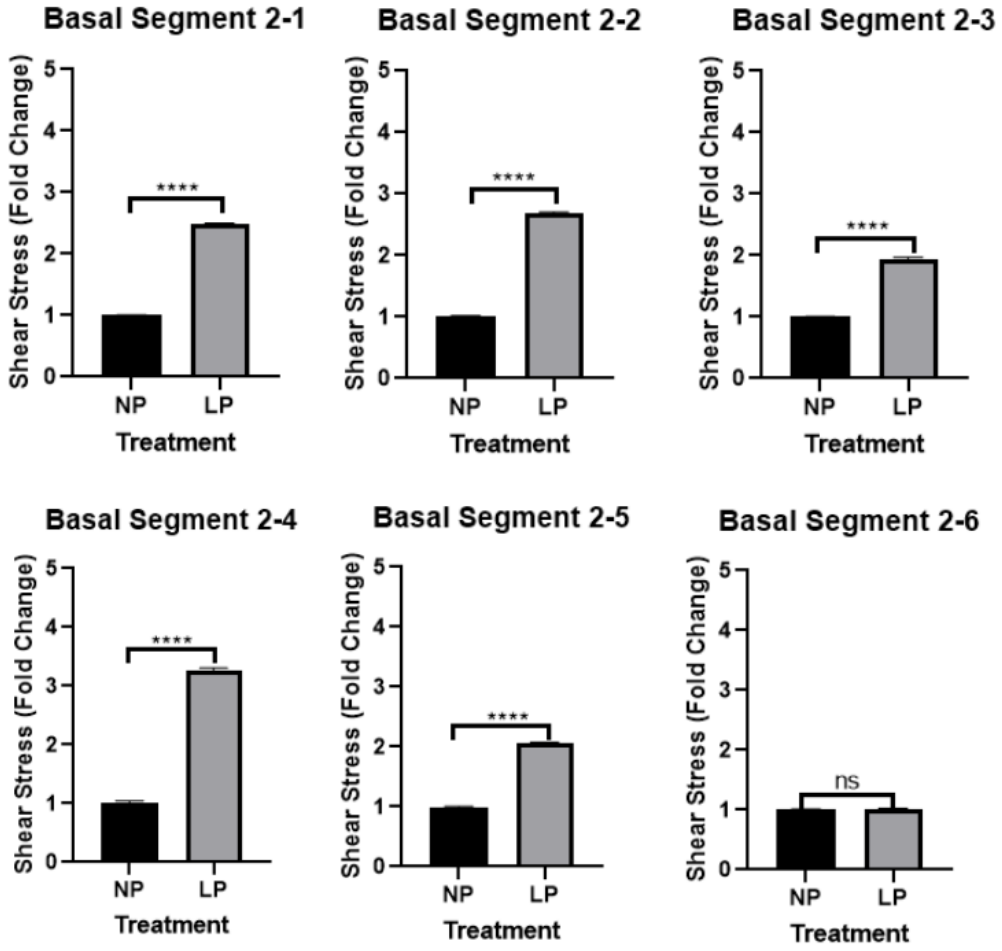

Fig. 5.12: T-test analysis for the second set of basal segments after comparing shear stress fold change between a no-pneumonectomy and a left pneumonectomy.

The shear stress and the shear stress fold change increase after a pneumonectomy vary between these six segments. There is a range from no observable change in the shear stress all to a 3-fold increase in the shear stress in these segments after a left pneumonectomy. For basal

segment 2-1, the original shear stress before the pneumonectomy was 120.27 dyne/cm^2 and after a left pneumonectomy, the shear stress in this segment increased to 299.57 dyne/cm^2. Basal Segment 2-2 experienced a significant change in the shear stress experienced on the artery wall after a pneumonectomy, as the shear stress increased from 134.68 dyne/cm^2 to 360.57 dyne/cm^2. Basal segment 3-3 had an original shear stress of 286.82 dyne/cm^2 prior to the pneumonectomy and this value increased to 557.43 dyne/cm^2 after a pneumonectomy. The largest increase in shear stress after a pneumonectomy occurred in basal branch segment 2-4, as the shear stress increased from 91.49 dyne/cm^2 to 289.67 dyne/cm^2 after a pneumonectomy. Basal branch segment 2-5 experienced an average shear stress of 181.26 dyne/cm^2 in the no-pneumonectomy model and this value increased to 373.42 dyne/cm^2 after the pneumonectomy. Basal branch segment 2-6 experienced only a slight change in shear stress between the no-pneumonectomy and pneumonectomy model, as the shear stress increased from 146.85 dyne/cm^2 to 148.36 dyne/cm^2. The T-test analysis for this segment determined that there was no significance between the shear stress before and after the pneumonectomy.

The right pneumonectomy resulted in changes in the shear stress on the left pulmonary artery and the basal branches that branch off the left artery. T-tests were performed for the remaining three main sections of the left pulmonary artery (LPA segment 1 was analyzed previously using an Anova analysis). Figure 5.13 displays the graphs that present the shear stress fold change for the left pulmonary artery segments 2 through 4 between the no-pneumonectomy and right pneumonectomy models, as well as the statistical significance in the change in shear stress.

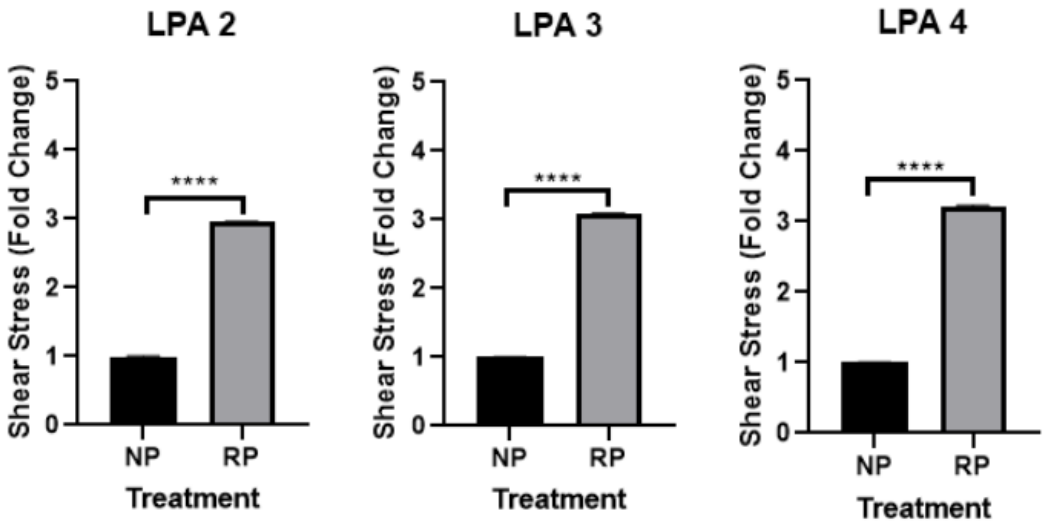

Fig. 5.13: T-test analysis for the left pulmonary artery segments after comparing shear stress fold change between a no-pneumonectomy and a right pneumonectomy.

As seen in Fig. 5.13, there was a significant difference in the shear stress fold change in all three sections of the left pulmonary artery after a right pneumonectomy. All three sections of the artery depicted above experienced approximately a three-fold increase in shear stress after a pneumonectomy. LPA segment 2 experienced a shear stress of 3.00 dyne/cm^2 in the no-pneumonectomy model, and after a right pneumonectomy the shear stress in this segment of the artery increased to 8.88 dyne/cm^2. LPA segment 3 originally experienced a shear stress of 3.03 dyne/cm^2 and after a pneumonectomy the shear stress increased to 9.35 dyne/cm^2. In LPA segment 4, the shear stress after a pneumonectomy increased from 9.46 dyne/cm^2 to 30.45 dyne/cm^2.

The left pulmonary artery also has two main groupings of basal branches that branch off the left pulmonary artery similar to the right pulmonary artery. T-test analyses for basal branch grouping 3, which consists of four different segments, were completed, and can be viewed in Fig. 5.14.

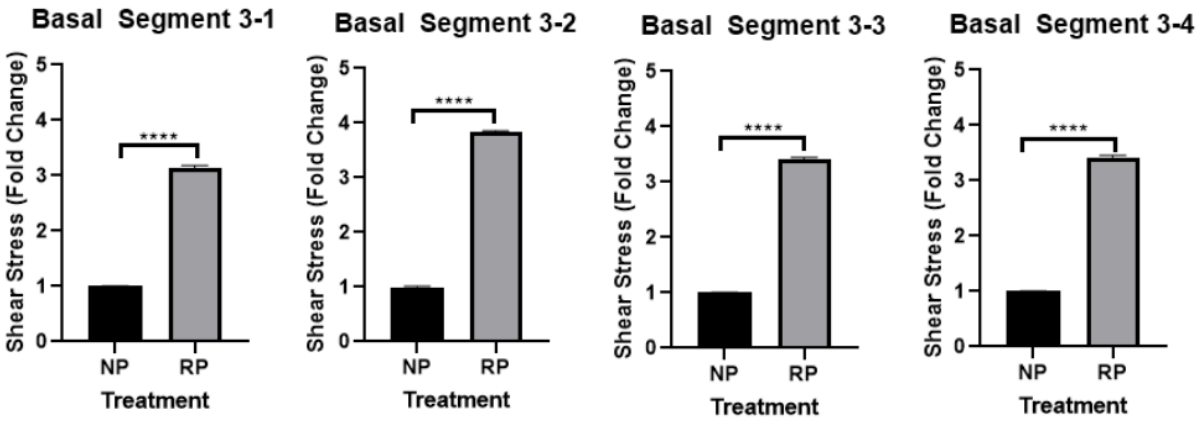

Fig. 5.14: T-test analysis for the third set of basal segments for comparing shear stress fold change between a no pneumonectomy and a right pneumonectomy.

This grouping of basal branches experienced the largest increases in the shear stress fold change after a pneumonectomy. Between the four segments, the average shear stress fold change was approximately 3.5 and this increase was significant for all four. Basal segment 3-1 originally experienced a shear stress of 13.91 dyne/cm^2 and after modeling a right pneumonectomy the shear stress increased to 43.71 dyne/cm^2. In basal segment 3-2, the shear stress was initially 38.52 dyne/cm^2, but increased to 147.59 dyne/cm^2 after a right pneumonectomy. Basal segment 3-3 had the largest increase and had high shear stress values compared to the other segments, which is possibly due to the smaller size of this segment. In the no-pneumonectomy model, the shear stress in the segment is 438.54 dyne/cm^2 and after a pneumonectomy this value increases to 1,493.05 dyne/cm^2. Basal branch segment 3-4 experienced a shear stress increase from 241.06 dyne/cm^2 to 825.62 dyne/cm^2.

The last grouping of basal branches also branches off the left pulmonary artery and is labeled as basal segments number 4. T-tests were utilized again to calculate the shear stress fold change between the no-pneumonectomy model and the right pneumonectomy model. Figure 5.15 demonstrates the shear stress fold change for the last four basal segments.

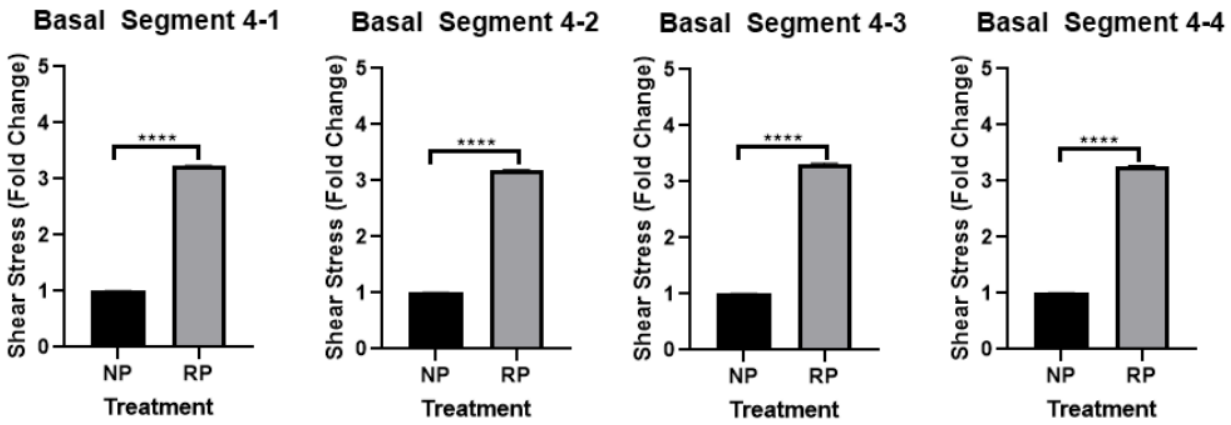

Fig. 5.15: T-test analysis for the fourth set of basal segments for comparing shear stress fold change between a no-pneumonectomy and a right pneumonectomy.

The shear stress fold change for the fourth grouping of basal segments is on average about a 3-fold change. As seen in Fig. 5.15 this increase in the shear stress fold change is significant for all four segments. For basal segment 4-1, the shear stress is originally at 61.76 dyne/cm^2 and after a pneumonectomy this value increases to 199.24 dyne/cm^2. For basal segment 4-2, the shear stress for the no-pneumonectomy model is 104.23 dyne/cm^2 and increases to 332.16 dyne/cm^2 after a pneumonectomy. Basal segment 3-3 had a relatively large shear stress value in the segment prior to a pneumonectomy at 343.95 dyne/cm^2, while after a pneumonectomy this value increased to 1,137.57 dyne/cm^2. Basal segment 4-4 originally experienced a shear stress of 264.60 dyne/cm^2 and after a pneumonectomy this value increased to 863.26 dyne/cm^2.

5.2 Biocompatibility Testing of Slides and Device

After the machining of the device for in-vitro experiments, biocompatibility testing had to be completed for the parallel plate flow chamber. Any part of the flow chamber that could potentially come in contact with the HLMVECs would have to be ensured that they are biocompatible; if there were any compatibility problems this could skew the results of the in vitro experiments. The three components of the parallel plate flow chamber that would come in contact with the HLMVECs were acrylic, Teflon, and glass slides. These components of the model were chosen for their known biocompatibility so it was hypothesized that no

biocompatibility problems would occur. The biocompatibility of the components was tested by seeding HLMVEC cells on each of these materials, then observing their proliferation and morphology. Once it had been demonstrated that the cells were not being affected by these materials, the components were deemed biocompatible and fit for their further use in the model for pneumonectomy experiments.

5.3 Verification of Controlled Fluid Flow & Mechanical Pump Calibration

The mechanical pump was calibrated by setting the desired flow direction, tube size, and flow rate. The same flow rate that was used for the experiments and fluid flow simulations was used in the calibration to ensure optimum accuracy. The adjusted flow rate of 171.6 mL/min was used to run the calibration and check the accuracy of the pump. A beaker of water was connected to the pump, and the other side of the pump was connected to a graduated cylinder to measure the volume. The mechanical pump was first primed to fill the tubing with water and any water that was pumped into the graduated cylinder was added back to the beaker source to ensure an accurate calibration process. The pump was then run to be calibrated at 171.6 mL/min to allow for the correct shear stress values. Once the pump had stopped, the amount of water in the graduated cylinder was measured and the value was entered into the tubing calibration volume on the pump. To ensure the pump was adjusted correctly, a second calibration was completed and was locked into the tubing calibration volume for future experiments.

5.4 Leak Testing

For data collection, the flow chamber design needs to be properly secured on all sides to prevent any leakage. Leakage can occur inside the chamber, at the chamber tubing connections, and at the tubing media container connections. To test for leakage, the 2D model was fully assembled. Using water as the test fluid, the device was attached to the pump, and the pump was set to begin at a low flow rate. When no leakage was observed, the flow rate was gradually increased to the desired experimental rate. When it was observed that still no leaking occurred, the leak testing stopped. This test was conducted three times, with each gasket in place, before progressing to experimental testing.

The first time the leak testing was performed there was quite a bit of leaking along the edges at the widest point where the gasket sits, to fix this, six more screws were added the center of the flow chamber as previously mentioned in the fabrication section. These extra screws in the center of the flow chamber allowed for the pressure to be more evenly distributed throughout the flow chamber and better seal the chamber. These screws proved successful in preventing leaking after reperforming the leak test for the no pneumonectomy model. The team found that for some of the pneumonectomy experiments there would be some slight leaks, but not always. The leaks were very minimal and adding c-clamps to the areas of leaking would fix the problem. The team was able to perform leak testing for each experiment type without leaking and determined that the device was working as intended.

5.5 Visualization of Cell Viability & Cell Staining

After completing in-vitro experiments, as previously mentioned the glass slides were removed from the flow chamber. The HLMVECs were fixed and then stained for confocal microscopy. The team was able to complete two experiments for each model type (2 experiments for the no pneumonectomy, 2 experiments for the right pneumonectomy, and 2 experiments for the left pneumonectomy). Unfortunately, due to time constraints only five of the six experiments were able to be imaged with the confocal microscope. Also, there was some damage to the glass slides during the experiment, so the team was only able to successfully analyze the cells for one experiment of each of the model types. All the images below were taken using a confocal microscope and the lenses corresponding to the DAPI and Alexa Fluor 488 stains were added to obtain images of the nuclei and glycocalyx layer. The images for the control, “no pneumonectomy” experiment can be seen in Fig. 5.16. In these images blue indicates the nuclei of the cell, and green indicates the glycocalyx.

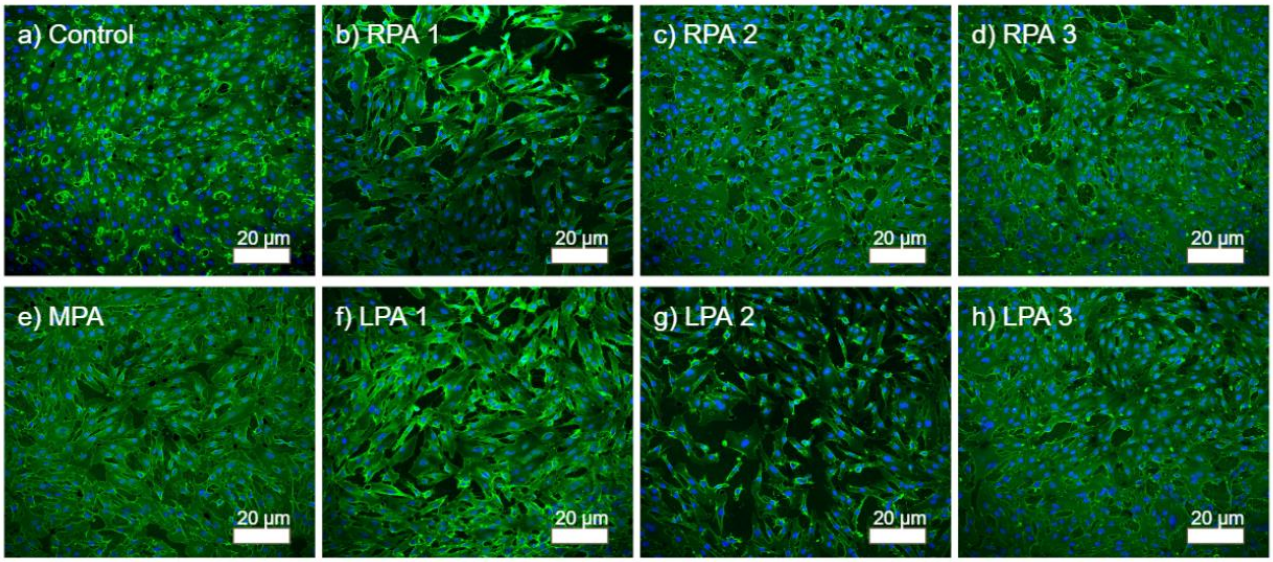

Fig. 5.16: These images are from the control; no pneumonectomy experiment slides. In these images the blue labels the nuclei and the green labels the glycocalyx. a) Is the control with no flow. b) is RPA testing point 1, c) is RPA testing point 2, and d) is RPA testing point 3. e) Is the first slide located in the MPA. f) Is LPA testing point 1, g) is LPA testing point 2, and h) is LPA testing point 3.

The no pneumonectomy images in Fig. 5.16, as anticipated, show a slight difference in visible coverage of the slides from the control or main pulmonary artery slides to the ones collected at the points in the right and left pulmonary arteries. This is intuitive as the flow is slightly restricted after these points due to the decrease in diameter of the chamber and angles of bifurcation. This increases the flow rate and shear stress on the cells slightly in these areas, thus affecting the cells.

Figure 5.17 shows the four images from the right pneumonectomy experiment. This experiment only includes the MPA, LPA 1, LPA 2, and LPA 3 as the right artery is blocked off for this experiment.

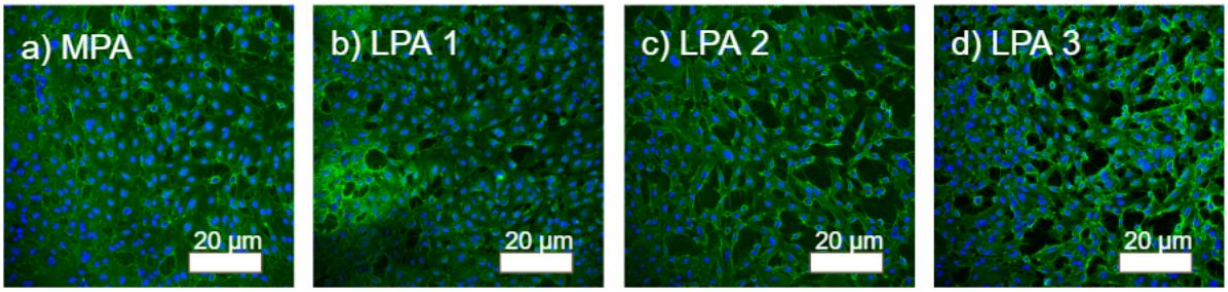

Figure 5.17: These images are of the right pneumonectomy slides. a) is the slide in the MPA. b) is LPA testing point 1, c) is LPA testing point 2, and d) is LPA testing point 3.

For a right pneumonectomy versus the control there should not be too much change in the MPA, but one would expect to see a change in the left pulmonary artery slides for a left pneumonectomy as the flow is blocked off from the right artery and is all forced through the left artery. As seen in Fig. 5.17 there is less coverage in LPA testing points 1 through 3 when compared to the MPA testing point.

Next, Fig. 5.18 shows the cell images from the left pneumonectomy which includes the glass slide from the main pulmonary artery as well as the three glass slides from the right pulmonary artery. Similar to the previous set of images, the glass slides from the left pulmonary artery are not included as the left artery is blocked off for this experiment.

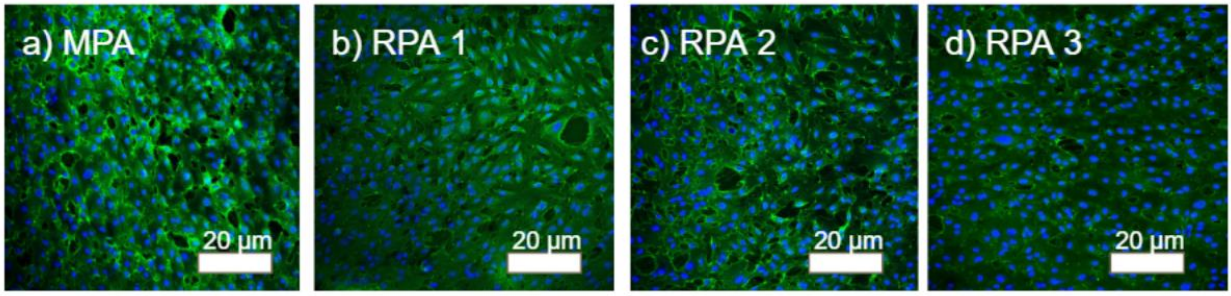

Fig. 5.18: These images are of the left pneumonectomy slides. a) is the slide in the MPA. b) is RPA testing point 1, c) is RPA testing point 2, and d) is RPA testing point 3.

Similar to the right pneumonectomy slides the team would expect that after a left pneumonectomy that there would be little change in the MPA glass slide, but more damage to the cells in the right pulmonary artery due to all the flow being forced down the one artery. This

would increase the shear stress and thus damage the HLMVECs. To quantify these results a coverage analysis and discontinuity of the endothelial layer analysis were completed.

5.5.1 Coverage Analysis

Using the software ImageJ, a coverage analysis was performed comparing the cell coverage between the control, "no pneumonectomy" cells and the pneumonectomy model cells. Fig. 5.19 compares the cell coverage between the control "no pneumonectomy" cells and the right pneumonectomy cells at the MPA, LPA 1 testing point, LPA 2 testing point, and LPA 3 testing point. A t-test was used to compare the coverage for each glass slide between the two experiments.

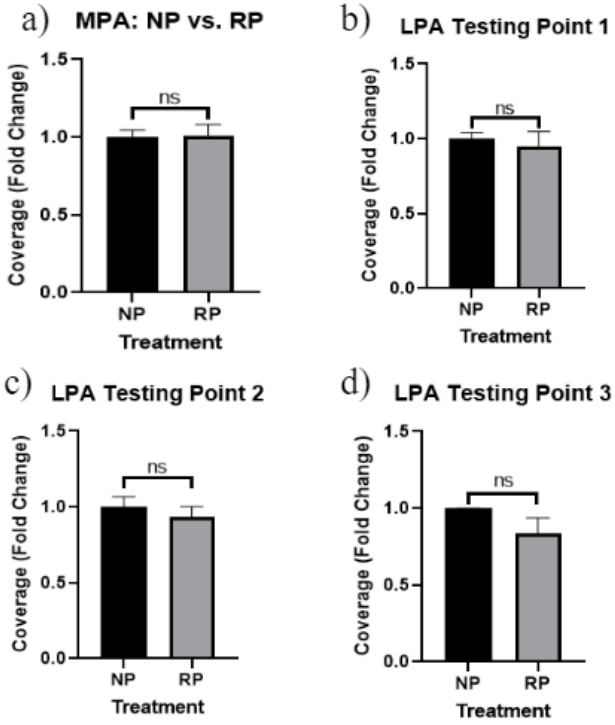

Fig. 5.19: T-test analysis of fold change coverage percentage between the control and right pneumonectomy experiment. a) MPA testing point, b) LPA testing point 1, c) LPA testing point 2, and d) LPA testing point 3.

While the graphs in Fig. 5.19 do show that there is a slight decrease in the fold change in the coverage percentage after a right pneumonectomy, there is no statistical significance at any

of the testing points. More experiments could potentially show a larger trend in this decrease in the cell coverage percentage and prove to be a significant change. The same analysis was then performed to compare the coverage between the control and the left pneumonectomy cell coverage and can be seen in Fig. 5.20.

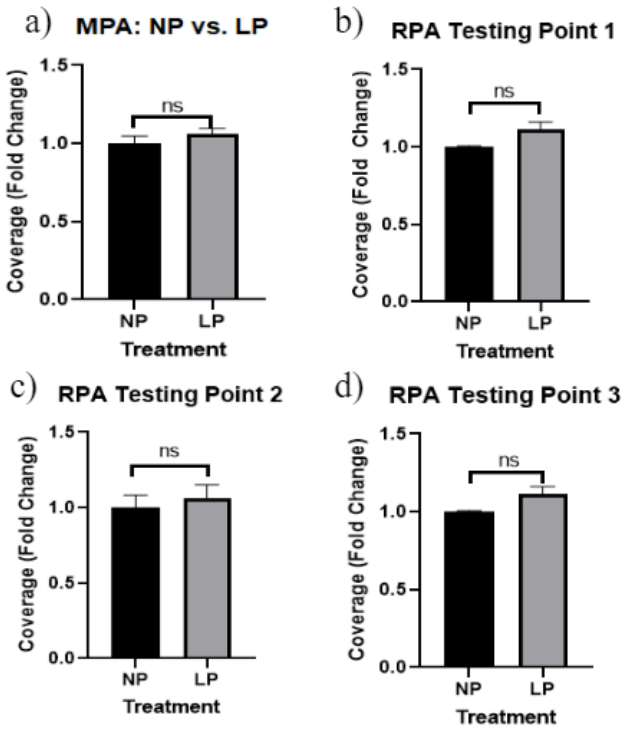

Fig. 5.20: T-test analysis of fold change coverage percentage between the control and left pneumonectomy experiment. a) MPA testing point, b) RPA testing point 1, c) RPA testing point 2, and d) RPA testing point 3.

The t-test analysis that compared the control and left pneumonectomy testing points also showed no significant difference in the coverage percentage fold change. Similar to the previous analysis this could be due to the few numbers of experiments that the team was able to run due to the time limitations of this project.

5.5.2 Discontinuity of the Endothelial Layer Analysis

An analysis was performed on the areas between the cell bodies and quantified using ImageJ to indicate cellular damage of the endothelial layer. The team hypothesized that the

discontinuity would increase after a pneumonectomy due to increased shear stress which would affect cellular functions and damage the proliferative capacity of the cells. The data analysis, however, demonstrated that there was no statistical significance in this presented in the images and can be seen in Fig. 5.21.

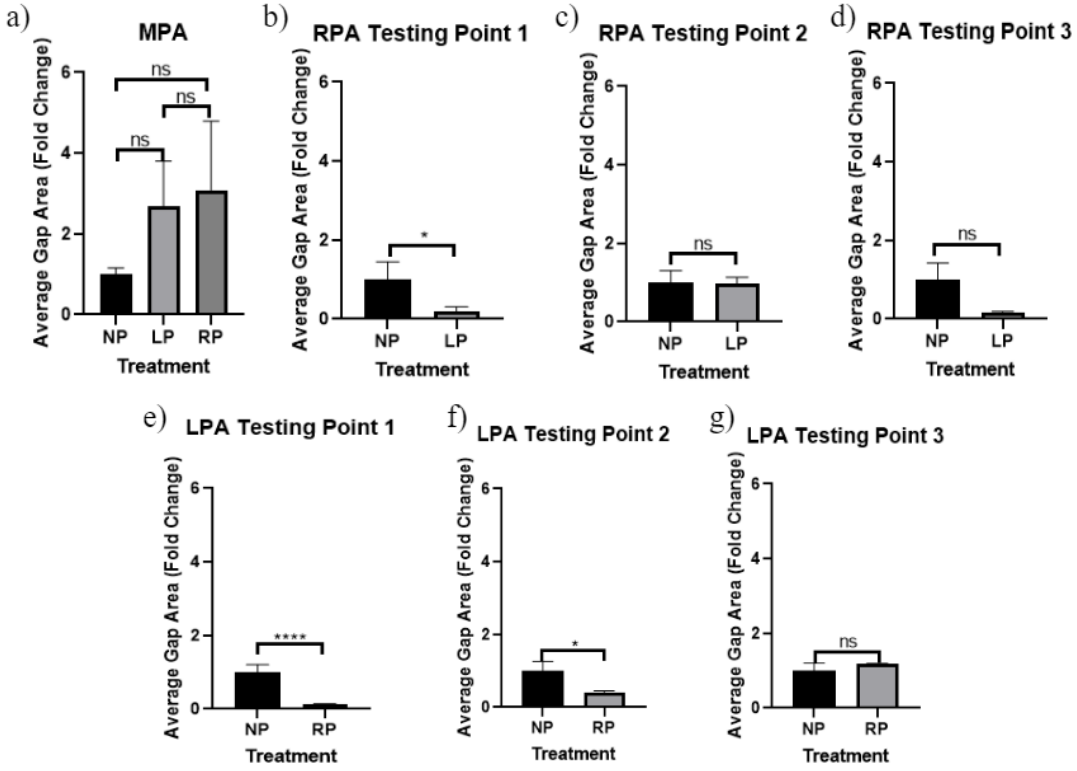

Fig. 5.21: Discontinuity of Endothelial layer statistical analysis. a) Anova analysis for MPA testing point, b) t-test for RPA testing point 1, c) t-test for RPA testing point 2, d) t-test for RPA testing point 3, e) t-test for LPA testing point 1, f) t-test for LPA testing point 2, and g) t-test for LPA testing point 3.

As seen in Fig. 5.21, testing point 3 for a right pneumonectomy (LPA) does indicate an increase in the area of gaps between the cells. However, the other points in both the models indicated decreases in discontinuity. It was observed that the data collected for the no pneumonectomy model indicated that there was a significantly larger than anticipated area of discontinuity of the endothelial layer. This was due to errors in the fixing and staining process which occurred after experimentation and affected the cell viability before the slides were able to be set and imaged. Additionally limited data was able to be collected due to time constraints. Comparisons between one experiment for both the right and left pneumonectomy was compared to one experiment for a control or no pneumonectomy model. Only having one data point for

each experimental model did not allow for a thorough analysis of the data to be performed. In the future more experiments would need to be conducted to collect more data, and procedures optimized to validate the hypothesis and prove significance in the data.

6. Final Design Validation

6.1 Recap of Goals

Throughout this project, the team worked towards meeting all four of the objectives to reach the overarching goal of understanding the effects of a pneumonectomy on the endothelial glycocalyx. To achieve the first objective, a literature review was performed to understand the problem and the pulmonary arteries themselves. Then, a 2D and 3D version of the pulmonary arteries were modeled using Solidworks. Flow simulations were completed for both models to understand blood flow patterns and changes in shear stress that occur after a pneumonectomy. Thorough data analysis and statistical analysis were completed using the flow simulation data. These flow simulations proved a significant increase in the shear stress after a pneumonectomy in the remaining artery. For the second objective, the 2D model became the parallel plate flow chamber, which was designed and manufactured. Multiple iterations and changes were made to the parallel plate flow chamber throughout the course of this project to ensure that accurate in-vitro experiments with HLMVECs would be able to be completed. The parallel plate flow chamber was then successfully machined for in-vitro testing. To meet the third objective, in-vitro experiments were completed for three model types which were the control (no-pneumonectomy), a left pneumonectomy, and a right pneumonectomy. This was done using the parallel plate flow chamber with HLMVECs seeded on glass slides inside of the flow chamber, and a mechanical pump that was used to introduce the desired flow into the system. This also required biocompatibility and leak testing to ensure that the flow chamber worked as intended. Finally, the team was able to complete the last objective by staining and imaging the cells from the in-vitro experiments. By imaging the cells, the team was able to measure confluency and coverage to determine the magnitude of damage that was caused to the endothelial glycocalyx due to the

increase in shear stress that occurs after a pneumonectomy. All the objectives that the team set out to complete were successfully completed throughout this project.

6.2 Economics

The parallel plate flow chamber designed and fabricated for this study could reduce or prevent the need for clinical trials and in-vivo testing regarding the effects of a pneumonectomy on the endothelial glycocalyx. In terms of patient costs, these in-vitro tests could, when analyzed in conjunction with a patient's medical record, provide information on the risk of complications involved with a pneumonectomy. It is in a patient's best interests to avoid complications resulting from any medical procedure, but a pneumonectomy can already be expensive at an average of $21,775, but this can increase by an average of $11,693 with just one complication sustained [40]. The costs associated with multiple complications and procedure-related deaths are even higher [40]. Through understanding the risks associated with having a pneumonectomy, medical professionals may be able to identify potential complications before a patient is harmed. Clinical trials also cost researchers a significant amount, such as when bringing a new drug to market, where they can cost on average $1335.9 million before success [41]. As a means of creating more resources for in-vitro testing regarding the effects of a pneumonectomy, devices such as the parallel plate flow chamber created here have the potential to reduce the costs associated with complications and in-vivo testing in clinical trials.

6.3 Environmental Impact

The parallel plate flow chamber designed and machined during this project is intended for repeated use. There should be little environmental impact as our product should only have to be manufactured once, the machining process creates minimal waste, and the device contains reusable parts. If the device were to be retired for unknown reasons, the materials used to create the flow chamber are plastics that can be recycled or reprocessed. This product should not have any intended negative impacts or effects on the environment with correct use of the device.

6.4 Ethical Concerns

When using a device to test human cell lines there are typically concerns with the ethicality of the acquisition of cell lines for this purpose. The ethical issues and challenges for human cell lines are usually disease and cell-type specific. The cell lines (HLMVECs) utilized in this study were sourced from the lungs of patients who had required procedures involving the removal or partial removal of a lung with Institutional Review Board approval obtained. Thus, there was no excess intended harm placed on donors undergoing these procedures.

Moreover, there should be no ethical concerns with the manufacturing or use of the device. The reusability of the device and potential use for reducing the necessity of in-vivo testing to model pneumonectomy conditions makes the device innoxious.

6.5 Health & Safety Issues

During experimentation, it was important that protocols were followed to maintain a safe and tidy work environment to prevent any health or safety hazards. The cell line used in the experiments, HLMVECs, does not pose any toxicity risk to humans themselves, however it is still important to ensure that policies are met to avoid any potential for risks [42]. The proper personal protective equipment (PPE) was worn at all times while working in the lab and was removed before using other equipment or leaving the lab to avoid contamination or risk of exposure to dangerous materials.

A sterile environment was maintained to avoid contamination of cell cultures and all work was performed using aseptic techniques in the sterile environment of a tissue culture hood. All glassware and plastics used for cell culture were opened in a sterile work environment and all other equipment related to the experiment, such as the tubing and device itself, were sterilized before use.

6.6 Manufacturability

While there is no need for it to be mass-produced, the parallel plate flow chamber can be easily replicated by others for repeating or conducting different experiments. The model has

three main components that require machining and a few other pieces required for assembly. To replicate the parallel plate flow chamber, either a mini-mill or a VM-2 CNC machine would be used to create the top and bottom plates of the parallel plate flow chamber. A laser cutter can also be used if needed to cut down larger pieces of acrylic to the general size desired. For the Teflon gaskets, the machining process is not as standardized as the top and bottom plates, but this process is still replicable. A bandsaw or similar tool should be used to cut down larger pieces of Teflon sheets into smaller sizes that are easier to work with. A VM-2 should be used to cut the Teflon pieces into the shape of the gaskets. The Teflon needs to be secured to a metal block to be placed into the machine. One way to do this is to put a layer of tape on the top of the metal sacrificial material, and on the bottom of the Teflon, and then glue the taped sides together. After the VM-2 has machined the shape of the gasket, the tape can be peeled up and removed. With knowledge of the use of this equipment, and the design specifications, the device is easily reproducible.

7. Discussion

The team was able to successfully complete all the set objectives for this Major Qualifying Project. Even when faced with constraints and limitations, the four original goals that the team set out to complete were achieved throughout this project. The team was successfully able to study the effects that pneumonectomy has on the endothelial glycocalyx. To understand the effects of this specific understudied procedure the team had to design a unique parallel plate flow chamber, specific to the needs of the team. By creating our own flow chamber, the team was able to include the unique flow path to mimic the pulmonary arteries as well as create any additional aspects that was needed for the specific needs of the project like our planned in-vitro experiments to further validate our findings. This project was also unique in the sense that the team was able to virtually study the shear stress at specific testing points not only for our designed parallel plate flow chamber, but also for an anatomically correct 3D version of the pulmonary arteries that was also created during this project.

The flow simulations on the designed parallel plate flow chamber used in this project indicate a significant increase in the shear stress after modeling a pneumonectomy. While this significant increase in shear stress is prevalent throughout the model it mostly seen in the remaining artery after modeling a pneumonectomy. The flow simulations which utilized the parallel plate flow chamber found that there was on average a three-fold increase in the shear stress magnitude on the endothelial cell slide indentations after a right pneumonectomy. It also determined that there is on average a four-fold increase in the shear stress magnitude on the cell slide spots after a left pneumonectomy.

The next stage in this project focused on flow simulations for a more anatomically correct 3D model. The 3D flow simulations found that after a right pneumonectomy there is about a four-fold increase in the shear stress in the main sections of the left pulmonary artery. After a left pneumonectomy, there is an average of a two and a half-fold increase in the shear stress magnitude in the main sections of the right pulmonary artery. Both the 2D and 3D flow simulations show that the shear stress at the majority of the testing points at least doubles after a pneumonectomy and that the increase is always statistically significant, but the 3D model demonstrates that a right pneumonectomy causes a greater increase in shear stress post pneumonectomy, and the 2D model demonstrates that a left pneumonectomy causes a greater

increase in shear stress post pneumonectomy. The 3D model flow simulations more accurately prove the findings in the literature review that a right pneumonectomy can result in more complications. These findings make sense as anatomically correct values were used to create the 3D model and when applying physiologically correct blood flow to the model the flow simulation analysis results in expected shear stress values found in the literature. Even though the flow simulations results vary between the 2D, and 3D model. The data collected from both models indicated that there is a significant increase in shear stress after one of the pulmonary arteries is blocked off.

Since the 3D model was intended to be a more accurate depiction of the pulmonary arteries, this model also includes the basal branch segments which were not studied in the 2D model. The newly added basal branches were broken into four different groupings. The first and second grouping of basal branches, which connect to the right pulmonary artery both experienced about a two-fold increase in the shear stress after a left pneumonectomy. Some of the individual segments experienced a greater shear stress fold change after a pneumonectomy and some experienced none. This is all relative to the dimension and angle of the specific branches. The third and fourth groupings of basal branches, which branch off the left pulmonary artery, experienced on average a 3.25-fold change in the shear stress after a right pneumonectomy.

Knowing about the significant increase in the shear stress after a pneumonectomy as well as the specific shear stress value that should be seen during the experiments, the team moved on to in-vitro experiments. The in-vitro experiments were hypothesized to provide the same percent increase in the shear stress after a pneumonectomy that was seen in the 2D flow simulations as the parallel plate flow chamber was being used. While some of the in-vitro experiments show the possibility of damage to the glycocalyx after a pneumonectomy, not enough experiments and cell analysis was completed to determine if the original hypothesis was met or not. This was due primarily to the limitation of time that the team had to complete the project.

While the parallel plate flow chamber was successfully fabricated and used for testing, the team ran into challenges during the fabrication of this model. First, the team experienced several issues regarding the machining of the parallel plate flow chamber that caused these processes to continue for longer than expected, which delayed the experimentation. For example,

experimentation was scheduled to take place immediately after the flow chamber was machined. However, the team experienced some significant problems with leakage in the flow chamber. This was remedied by adding Teflon tape to the bottom plate, manually sanding down the gaskets with sandpaper to improve the fit, adding more screws to the model to distribute pressure more evenly, and even using some c-clamps for some experiments to help prevent the leaking. This issue prevented experiments from being completed for about two weeks. Another limitation with the in-vitro testing of the parallel plate flow chamber was that the glass slides used in experiments were small and fragile, resulting in some breaking or otherwise becoming damaged during experimentation. This fragmentation allowed the slide sealant, nail polish, to be absorbed under the slide and affect the staining, observable as the dark or cloudy regions. This also could have affected the cell viability before fixing was completed.

Due to the long length of time it takes to complete one experiment and the limited availability of the mechanical pump needed for experiments, the team was only able to perform six experiments. Our original goal was to complete nine experiments which would be three experiments for each model type (no pneumonectomy, right pneumonectomy, and left pneumonectomy), but due to this limitation we were only able to complete two of each. Another limitation was the imaging of our samples. While the team was able to stain the nuclei and glycocalyx for the glass slides for all six of our completed experiments, only the cells from five of these experiments were able to be imaged. This was due to the large amount of glass slides the team needed to be imaged per experiment (either 5 or 8 glass slides depending on the experiment) and the limited time that the team had access to the confocal microscope. Due to the limited time with the confocal, the team was also unable to perform z-stack images in the orthogonal view to measure the thickness of the glycocalyx. That is why the team recommends the continuation of this project to complete these unfinished goals.

Lastly, the team found that there would not be enough time to create both a 2D and 3D model of the pulmonary arteries both virtually and for in-vitro testing. Due to the limitation of time, the team had to abandon the fabrication of a 3D model for in-vitro testing. While the team did run into numerous limitations during the courses of this project, a successful parallel plate flow chamber was designed, created, and tested in the brief time frame. The flow simulations for both the 2D and 3D models provide valuable data about the changes in flow, pressure, and shear

stress that can occur after a pneumonectomy. Even with the limitations of these devices, as they are designed as rigid bodies and the 2D model only focuses on the bifurcation point, this data is a step in the right direction for understanding changes after a pneumonectomy that can affect the glycocalyx layer. Also, in-vitro experiments were successfully designed and ran as intended which allowed for the collection of further cell analysis data. While more experiments and cell analysis need to be completed to make a statement on the hypothesis, trends in the coverage that favored our hypothesis were observed.

8. Conclusion & Recommendations

Throughout the two versions of virtual flow simulations and the in-vitro testing, the team concludes that for both of our models the shear stress magnitude on the endothelial glycocalyx increases significantly after modeling a pneumonectomy. While more in-vitro experiments and in-vivo experiments would have to be completed to fully confirm our hypothesis, the team has made great strides in better understanding the change in flow pattern, shear stress, and glycocalyx damage that can occur after a pneumonectomy. Future work surrounding this project includes the continued use of the parallel plate flow chamber created during this project. More data and cell analyses can be performed to validate the findings of this project as well as additional imaging of the cells. Performing z-stacks with the confocal microscope would allow for the orthogonal view to be observed and measured to indicate the thickness changes of the glycocalyx under pneumonectomy flow changes. Other future work for this project includes the fabrication of the 3D model that was designed in Solidworks, as well as the completion of in-vitro experiments using this model. Many complications and questions arise when determining how to fabricate a 3D model to run in-vitro experiments with. Future work would include the testing of materials used to create 3D versions of the pulmonary arteries that would prevent fluid from leaking. Another aspect of this future work would be to determine how to introduce the HLMVECs into the 3D model for flow simulations and afterwards determine a way to remove and image them. Developing and optimizing a process using the 3D model would allow for the most accurate measurements of the cellular changes under pneumonectomy conditions to be measured and analyzed. This would serve to further justify the explanations to conditions that occur following a pneumonectomy procedure.

References

[1] E. J. Chae et al., "Radiographic and CT findings of thoracic complications after pneumonectomy," RadioGraphics vol. 26, no. 5, pp. 1149-1468, 2006, doi: https://doi.org/10.1148/rg.265055156.

[2] D. R. Hall, "Regional lung function after pneumonectomy," BMJ Journals, vol. 29, no. 4, pp. 425-431, 1974, doi: http://dx.doi.org/10.1136/thx.29.4.425.

[3] C. J. Yang et al., "Right-Sided Versus Left-Sided Pneumonectomy After Induction Therapy for Non-Small Cell Lung Cancer," The Annals of Thoracic Surgery, vol. 107, no. 4, April 2019, doi: https://doi.org/10.1016/j.athoracsur.2018.10.009.

[4] A. Kandathil and M. Chamarthy, "Pulmonary vascular anatomy & anatomical variants," Cardiovascular Diagnosis & Therapy, vol. 8, no. 3, pp. 201–207, June 2019, doi: https://doi.org/10.21037/cdt.2018.01.04.

[5] M. I. Townsley, "Structure and Composition of Pulmonary Arteries, Capillaries, and Veins," Comprehensive Physiology, vol. 2, no. 1, pp. 675–709, January 2012, doi: https://doi.org/10.1002/cphy.c100081.

[6] "How the Lungs Work." Temple Health. https://www.templehealth.org/services/lung/patient-care/patient-resources/understanding-lung-disease/how-lungs-work (accessed December 2021).

[7] U. Joseph Schoepf and J. F. M. Meaney. "Pulmonary Vasculature." https://thoracickey.com/pulmonary-vasculature/ (accessed.

[8] U Bozlar et al., "Pulmonary artery diameters measured by multidetector-row computed tomography in healthy adults," Acta Radiol, vol. 48, no. 10, pp. 1086 - 1091, Dec 2007, doi: 10.1080/02841850701545755.

[9] M. Ramella et al., "Effect of Cyclic Stretch on Vascular Endothelial Cells and Abdominal Aortic Aneurysm (AAA): Role in the Inflammatory Response," International Journal of Molecular Sciences, vol. 20, no. 2, p. 287, 2019, doi: https://doi.org/10.3390/ijms20020287.

[10] S. Dogné, B. Flamion, and N. Caron, "Endothelial Glycocalyx as a Shield Against Diabetic Vascular Complications," Arteriosclerosis, Thrombosis, and Vascular Biology, vol. 38, no. 7, pp. 1427–1439, 2018, doi: https://doi.org/10.1161/ATVBAHA.118.310839.

[11] C.S. Alphonsus, R. N. Rodseth, "The Endothelial Glycocalyx: a Review of the Vascular Barrier." Anaesthesia, vol. 69, no. 7, Wiley Subscription Services, Inc, 2014, pp. 777–84, https://doi.org/10.1111/anae.12661.

[12] G. Wang et al., "Shear Stress Regulation of Endothelial Glycocalyx Structure Is Determined by Glucobiosynthesis," Arteriosclerosis, Thrombosis, and Vascular Biology, vol. 40, no. 2, pp. 350–364, 12 Dec 2019, doi: https://doi.org/10.1161/ATVBAHA.119.313399.

[13] J. W. VanTeeffelen, J. Brands, E. S. Stores, and H. Vink, "Endothelial Glycocalyx: Sweet Shield of Blood Vessels," Trends in Cardiovascular Medicine, vol. 17, no. 3, pp. 101-105, 2007, doi: https://doi.org/10.1016/j.tcm.2007.02.002.

[14] A. Koo, C. F. Dewey Jr., and G, Garcia-Cardena, "Hemodynamic shear stress characteristic of atherosclerosis-resistant regions promotes glycocalyx formation in cultured endothelial cells," American Journal of Physiology Cell Physiology vol. 304, no. 2, pp. C137–C146., 2013, doi: https://doi.org/10.1152/ajpcell.00187.2012.

[15] M. Nieuwdorp, H. L. Mooij, J. Kroon, and A. Bektas, "Endothelial Glycocalyx Damage Coincides with Microalbuminuria in Type 1 Diabetes." Diabetes: Retinal Conditions (in Spanish), vol. 55, Ebix Inc, 2006, pp. 1127–32.

[16] S. Reitsma, D.W. Slaaf, H. Vink, M. A. M. J. vanZandvoort, and M. G. A. Oude Egbrink, "The Endothelial Glycocalyx: Composition, Functions, and Visualization." Pflügers Archiv : European Journal of Physiology., vol. 454, Springer-Verlag, 2007, pp. 345–59.

[17] Rancan L. et al., "Glycocalyx Degradation after Pulmonary Transplantation Surgery," European Surgical Research, vol. 59, pp. 115–125, 2018, doi: https://doi.org/10.1159/000489492.

[18] F. Vannucci, A. Vieira, and U. Paula A, "The technique of VATS right pneumonectomy," Journal of Visualized Surgery vol. 4, 2018, doi: 10.21037/jovs.2017.12.01.

[19] "Pneumonectomy Surgery for Mesothelioma , Defeated Lung Removed." CleverBoris. https://cleverboris.blogspot.com/2016/03/pneumonectomy-surgery-for-mesothelioma.html (accessed.

[20] N. Todorovic. "Left pneumonectomy." https://radiopaedia.org/cases/left-pneumonectomy (accessed.

[21] C.-L. Bennin, "Post-Pneumonectomy Changes," The Medicine Forum:, vol. 12, no. 21, 2010, doi: https://doi.org/10.29046/TMF.012.1.020

[22] J. Deslauriers et al., "Adjustments in cardiorespiratory function after pneumonectomy: Results of the pneumonectomy project," vol. 141, no. 1, pp. 7-15, January 2011, doi: https://doi.org/10.1016/j.jtcvs.2010.09.010.

[23] L. M. Brown, S. R. Rannels, and D. E. Rannels, "Implications of post-pneumonectomy compensatory lung growth in pulmonary physiology and disease," Respiratory Research, vol. 2, no. 6, pp. 340-347, 2001, doi: . https://doi.org/10.1186/rr84.

[24] I. Bazwinsky-Wutschkea, F. Paulsen, D. Stövesandt, H.-J. Holzhausen, H.-J. Heinea, and E. Peschkea, "Anatomical changes after pneumonectomy," Annals of Anatomy - Anatomischer Anzeiger, vol. 193, no. 2, pp. 168-172, March 2011, doi: https://doi.org/10.1016/j.aanat.2011.01.002.

[25] N. Rol et al., "Vascular remodelling in the pulmonary circulation after major lung resection," European Respiratory Journal, vol. 50, no. 2, p. 1700806., 2017, doi: 10.1183/13993003.00806-2017.

[26] J. D. Crouch, C. L. Lucas, B. A. Keagy, B. R. Wilcox, and H. Belinda, "The Acute Effects of Pneumonectomy on Pulmonary Vascular Impedance in the Dog," The Annals of Thoracic Surgery, vol. 43, no. 6, pp. 613-616, June 1987, doi: https://doi.org/10.1016/S0003-4975(10)60231-7.

[27] K. Sato, M. Nitta, and A. Ogawa, "A Microfluidic Cell Stretch Device to Investigate the Effects of Stretching Stress on Artery Smooth Muscle Cell Proliferation in Pulmonary Arterial Hypertension," Inventions, vol. 4, no. 1, p. 1, 26 December 2018, doi: https://doi.org/10.3390/inventions4010001.

[28] B.J Chung, A.M Robertson, and D. G. Peters, "The numerical design of a parallel plate flow chamber for investigation of endothelial cell response to shear stress," Computers & Structures, vol. 81, no. 8-11, pp. 535-546, May 2003, doi: https://doi.org/10.1016/S0045-7949(02)00416-9.

[29] A. K. Wong, P. L. Lanos, N. Boroda, S. R. Rosenberg, and S. Y. Rabbany, "A Parallel-Plate Flow Chamber for Mechanical Characterization of Endothelial Cells Exposed to Laminar Shear Stress," Cellular and Molecular Bioengineering, vol. 9, pp. 127-138, 27 October 2015, doi: https://doi.org/10.1007/s12195-015-0424-5.

[30] Association for the Advancement of Medical Instrumentation & American National Standards Institute, 2009. [Online]. Available: https://www.iso.org/obp/ui#iso:std:iso:10993:-5:ed-3:v1:en

[31] M.-J. Chern, M.-T. Wu, and S.-W. Her, "Numerical Study for Blood Flow in Pulmonary Arteries after Repair of Tetralogy of Fallot," Hindawi, vol. 2012, no. 198108, 27 Dec 2012, doi: https://doi.org/10.1155/2012/198108.

[32] C. Kriesi, M. Steinert, A, Marmaras, C. Danzer, V. Meskenaite, and V. Kurtcuoglu, "Integrated Flow Chamber System for Live Cell Microscopy," Frontiers in bioengineering and biotechnology, 01 May 2019, doi: https://doi.org/10.3389/fbioe.2019.00091.

[33] E. Finol. "Pulmonary arteries (human)." https://www.thingiverse.com/thing:93932

[34] "DOW SYLGARD™ 184 SILICONE ENCAPSULANT CLEAR 0.5 KG KIT." https://www.ellsworth.com/products/by-market/consumer-products/encapsulants/silicone/dow-sylgard-184-silicone-encapsulant-clear-0.5-kg-kit/ (accessed December 19, 2021).

[35] E. McGovern, C. Voss, N. W. Brunner, S. Duncombe, K. C. Harris, and M. H. Hosking, "Pulmonary artery wall thickness in children with Fontan physiology: an optical coherence tomography case control study," Cardiology in the Young, vol. 29, no. 4, pp. 524-527, 08 April 2019, doi: https://doi.org/10.1017/s1047951119000362

[36] J. W. Kim and J.-H. Chang, "Syntheses of Colorless and Transparent Polyimide Membranes for Microfiltration," Polymers, vol. 12, no. 7, p. 1610, 20 July 2020, doi: https://doi.org/10.3390/polym12071610.

[37] H. A. Strobel, E. L. Calamari, T. A. Hookway, and M. W. Rolle, "Fabrication of Custom Agarose Wells for Cell Seeding and Tissue Ring Self-assembly Using 3D-Printed Molds," Journal of Visualized Experiments, vol. 134, April 2, 2018, doi: 10.3791/56618.

[38] J. King and D. R. Lowery, "Physiology, Cardiac Output," National Library of Medicine: StatPearls, January 2022. [Online]. Available: https://www.ncbi.nlm.nih.gov/books/NBK470455/.

[39] W. Salibe-Filho et al., "Shear stress-exposed pulmonary artery endothelial cells fail to upregulate HSP70 in chronic thromboembolic pulmonary hypertension," PLOS ONE, vol. 15, no. 12, 3 December 2020, doi: https://doi.org/10.1371/journal.pone.0242960

[40] J. R. Handy Jr, K. Denniston, G. L. Grunkemeier, and Y. X. Wu, "What Is the Inpatient Cost of Hospital Complications or Death After Lobectomy or Pneumonectomy?," The Annals of Thoracic Surgery, vol. 91, no. 1, pp. 234-238, January 2011, doi: https://doi.org/10.1016/j.athoracsur.2010.08.043.

[41] O. J. Wouters, M. McKee, and J. Luyten, "Estimated Research and Development Investment Needed to Bring a New Medicine to Market, 2009-2018," JAMA, vol. 323, no. 9, pp. 844-853, 3 March 2020, doi: doi:10.1001/jama.2020.1166.

[42] (2021). HMVEC-L - Human Lung Microvascular Endothelial Cells. [Online] Available: https://bioscience.lonza.com/lonza_bs/US/en/p/PDFdocument?productCode=000000000000184961&reptype=MSDS&rvlid=US&iso=EN

Appendix A: List of Expenses

Item	Specifications	Use	Quantity	Total Price
Acrylic Sheets	Clear Scratch & UV-Resistant Cast Acrylic Sheets 6” x 12” x ½” McMasterCarr (8560K279)	Top & Bottom Plate of Flow Chamber	2	$39.30
Teflon	Chemical-Resistant Slippery Teflon PTFE Sheet White, 1/16” Thick, 12” Wide, 12” Long McMasterCarr (8545K22)	Used to make the 3 Gaskets	1	$51.47
Dowel Pins	4037, 4140 Alloy Steel, ⅛” Diameter, 1-⅜” Long McMasterCarr (98391A494)	Bought to line up plates, but was not needed	1 Pack (Contains 5)	$3.29
Bolts	18-8 Stainless Steel Hex Head Screw 5/16” - 18 Thread Size, 1” Long McMasterCarr (92240A583)	Used to hold two plates together, but got replaced by screws	1 Pack (Contains 25)	$6.58
Screws	18-8 Stainless Steel Pan Head Slotted Screws	Used to hold two plates together	1 Pack (Contains 25)	$14.04

	5/16” - 18 Thread Size, 1” Long McMasterCarr (91792A583)			
Silicone	Smooth-On OOMOO 30 Silicone Moldmaking Rubber (Pint Unit)	Fabrication testing of 3D Model	1 (1 pint unit)	$32.75
PVA Filament	PVA Printer Filament, Degradable and Dissolves 3D Printing Filament 1.75mm Dimensional Accuracy +/- 0.05 mm, 0.5kg Spool, Natural Color	Fabrication testing of 3D Model	1 (0.5 kg spool)	$34.56
Tubing	Masterflex L/S®Precision Pump Tubing, BioPharm Platinum-Cured Silicone, L/S 25; 25ft	Connect mechanical pump to flow chamber	1 Pack (25 ft)	$188.00
Culture Medium	Microvascular Endothelial Cell Growth Medium (111-500) (Sigma-Aldrich)	For cell culture	1 (500mL)	$161.00
Flash Drive	SanDisk 64GB Cruzer USB 2.0 Flash Drive - SDCZ36-064G-B35	For Cell Imaging & To Transfer all our work too	1	$11.29
Primary Antibody	Wheat Germ Agglutinin (WGA), Biotinylated	Cell Staining	1	$194

	B-1025-5			
Secondary Antibody	Streptavidin, Alexa Fluor™ 488 conjugate Catalog number: S11223	Cell Staining	1	$273
Total Spent				$1,009.28
Amount Remaining				$240.72

Appendix B: ImageJ Analysis of Discontinuity of the Endothelial Layer

1) Open ImgaeJ Software > Open image file of interest
2) Go to “Image” > “color” > “Split Channels.” Select the channel that shows the endothelial cell layers and excludes the nuclei (the GFP channel).
3) Go to “Image” > “Adjust” > “Threshold” > Select Red filter. Adjust the values until the cell bodies appear in gray or black and the gaps appear red.
4) Go to “Analyze”> “Analyze Particles.” Select “Display Results,” “Clear Results,” “Include holes,” and “Add to Manager,” unselect “Exclude on edges.” Select from drop down “Outlines,” and do not adjust automatic settings for “Circularity” (0.01-1.00), and “Size” (0-infinity).
5) A new image and a results table with the Area, Mean, Min, and Max values for the selected regions with be given. This can be exported to Excel by saving the file.

Appendix C: ImageJ Analysis of Coverage

1) Open ImageJ Software > Open file image

2) When the file opens a new screen will appear, Select the following options:

- View Stack with – Hyperstack

- Color Mode – Colorized

Press “Okay”

3) A second screen will appear with individual images, make sure that there are many planes then select the image of choice, and hit “Okay”

4) Go to “Image” > “Color” > “Make Composite”

5) Go to “Image” > “Color” > “Split Channels”

6) Select the green image, then go to “Image” > “Adjust” > “Color Balance” on the settings, select “green” and move the cursor for the maximum about a third of the way down, and adjust until the green is appears brighter. Hit “Apply” then adjust the cursor again before hitting “Apply” a second time. Move the minimum cursor to reduce the haze, “Apply,” then adjust a second time, “Apply”

7) Go to “Image” > “Adjust” > “Threshold” Adjust the threshold window so that the red more accurately represents the glycocalyx. Record the percentage, as that will be the coverage value.

Appendix D: Cell Culture Protocol

A. Preparing Cell Culture Flasks for Culturing HLMVEC
    a. Take the Microvascular Endothelium Cell Growth Medium (111-500) from the refrigerator. Place it in a 37°C water bath for 20 minutes. Decontaminate the bottle with 70% alcohol and place the bottle in a sterile hood.
    b. Prepare T-25 Flask by pipetting 8mL of Microvascular Endothelium Cell Growth Medium into the flask.

B. Thawing and Plating HLMVEC
    a. Remove the cryopreserved vial of HLMVEC from liquid nitrogen and place the vial in a 37°C water bath for a few minutes. Watch closely and when there is a little ice left in the vial remove from water bath. Decontaminate the bottle with 70% alcohol and place the bottle in a sterile hood.
    b. Carefully remove the cap of the vial and resuspend the cells by gently pipetting back and forth. Remove the cap of the T-25 Flask.
    c. Pipette the contents of the vial into a T-25 Flask with 8mL of Microvascular Endothelium Cell Growth Medium. Place the cap back on and place the flask in an incubator at 37°C, 5% CO2.
    d. After 24 hours, change the media. Then continue to change the media every other day until cell confluency.

C. Subculturing HLMVEC and Plating HLMVEC for use in Experiments
    a. Place Trypsin into a 37°C water bath for 20 minutes. Decontaminate the bottle with 70% alcohol and place the bottle in a sterile hood.
    b. Take T-25 Flask with HLMVEC and place in sterile hood.
    c. Aspirate away the media in the flask. Pipette 1mL of Trypsin in the flask and then aspirate it away. Pipette an additional 2 mL of Trypsin in the flask and wait for 5 minutes. Check the flask under a microscope, cells should be rounded. Gently tap the flask to detach the cells. Check again under the microscope. Once all cells are detached pipette 6 mL of Microvascular Endothelium Cell Growth Medium into the flask.
    d. Pipette back and forth, then transfer the cell suspension into a 15 mL conical tube.
    e. Centrifuge the conical tube for 5 minutes at 200 xG to pellet the cells.

f. Aspirate the supernatant from the tube, careful not to disturb the cell pellet.
g. Pipette 4 mL of Microvascular Endothelium Cell Growth Medium into the conical tube, and gently pipette back and forth to resuspend the cells.
h. Count the cells with a hemocytometer. Add 20,000 cells to each 10mmx10mm glass slide in a petri dish. Place in incubator for 30 minutes.
i. Pipette remaining cell suspension into new T-25 Flask with 8mL of Microvascular Endothelium Cell Growth Medium. Then place the flask in an incubator at 37°C, 5% CO2. Change media every other day until confluent.
j. After 30 minutes, pipette 2 mL of Microvascular Endothelium Cell Growth Medium into each petri dish. Then place the petri dishes back in the incubator. These will be ready for use in experiments the next day.